Outskirts of Distant Galaxies In Absorption

Hsiao-Wen Chen

Abstract QSO absorption spectroscopy provides a sensitive probe of both the neutral medium and diffuse ionized gas in the distant Universe. It extends 21 cm maps of gaseous structures around low-redshift galaxies both to lower gas column densities and to higher redshifts. Combining galaxy surveys with absorption-line observations of gas around galaxies enables comprehensive studies of baryon cycles in galaxy outskirts over cosmic time. This Chapter presents a review of the empirical understanding of the cosmic neutral gas reservoir from studies of damped Lyα absorbers (DLAs). It describes the constraints on the star formation relation and chemical enrichment history in the outskirts of distant galaxies from DLA studies. A brief discussion of available constraints on the ionized circumgalactic gas from studies of lower column density Lyα absorbers and associated ionic absorption transitions is presented at the end.

1 Introduction

Absorption-line spectroscopy complements emission surveys and provides a powerful tool for studying the diffuse, large-scale baryonic structures in the distant Universe (e.g., Rauch 1998; Wolfe et al 2005; Prochaska and Tumlinson 2009). Depending on the physical conditions of the gas (including gas density, temperature, ionization state, and metallicity), a high-density region in the foreground is expected to imprint various absorption transitions of different line strengths in the spectrum of a background QSO. Observing the absorption features imprinted in QSO spectra enables a uniform survey of diffuse gas in and around galaxies, as well as detailed studies of the physical conditions of the gas at redshifts as high as the background sources can be observed.

Hsiao-Wen Chen
Department of Astronomy & Astrophysics, and Kavli Institute for Cosmological Physics, The University of Chicago, Chicago, IL 60637, USA, e-mail: hchen@oddjob.uchicago.edu

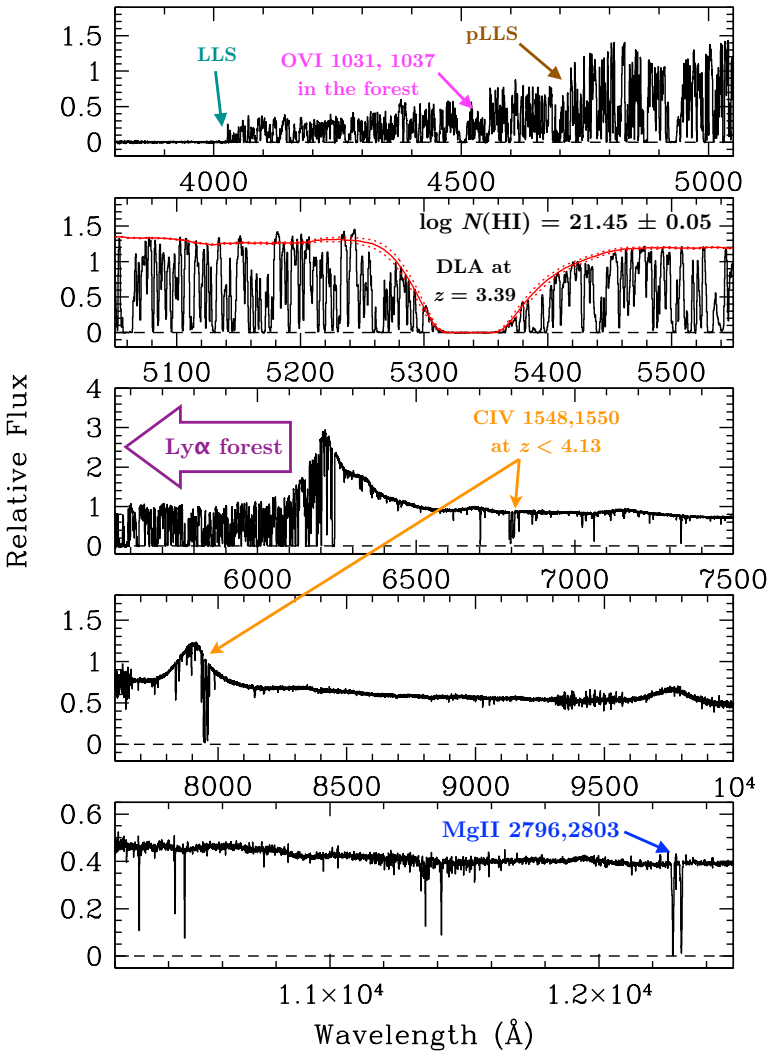

Fig. 1 Example of the wealth of information for intervening gas revealed in the optical and near-infrared spectrum of a QSO at $z = 4.13$. In addition to broad emission lines intrinsic to the QSO, such as Lyα/N V at ≈ 6200 Å, a forest of Lyα λ 1215 absorption lines is observed blueward of 6200 Å. These Lyα forest lines arise in relatively high gas density regions at $z_{\rm abs} \lesssim z_{\rm QSO}$ along the line of sight. The Lyα absorbers span over 10 decades in neutral hydrogen column densities (N(H I)), and include (1) neutral damped Lyα absorbers (DLAs), (2) optically thick Lyman limit systems (LLS), (3) partial LLS (pLLS), and (4) highly ionized Lyα absorbers (see text for a quantitative definition of these different classes). The DLAs are characterized by pronounced damping wings (*second panel from the top*), while LLS and pLLS are identified based on the apparent flux discontinuities in QSO spectra (*top panel*). Many of these strong Lyα absorbers are accompanied with metal absorption transitions such as the O VI $\lambda\lambda$ 1031, 1037 doublet transitions which occur in the Lyα forest, and the C IV $\lambda\lambda$ 1548, 1550 and Mg II $\lambda\lambda$ 2796, 2803 doublets. Together, these metal lines constrain the ionization state and chemical enrichment of the gas

Figure 1 displays an example of optical and near-infrared spectra of a high-redshift QSO. The QSO is at redshift $z_{\rm QSO} = 4.13$, and the spectra are retrieved from the XQ-100 archive (Lopez et al 2016). At the QSO redshift, multiple broad emission lines are observed, including the Lyα/N V emission at ≈ 6200 Å, C IV emission at ≈ 7900 Å, and C III] emission at ≈ 9800 Å. Blueward of the Lyα emission line are a forest of Lyα λ 1215 absorption lines produced by intervening overdense regions at $z_{\rm abs} \lesssim z_{\rm QSO}$ along the QSO sightline. These overdense regions span a wide range in H I column density (N(H I)), from neutral interstellar gas of $N({\rm H\,I}) \geq 10^{20.3}\,{\rm cm}^{-2}$, to optically opaque Lyman limit systems (LLS) of $N({\rm H\,I}) > 10^{17.2}\,{\rm cm}^{-2}$, to optically thin partial LLS (pLLS) with $N({\rm H\,I}) = 10^{15-17.2}\,{\rm cm}^{-2}$, and to highly ionized Lyα forest lines with $N({\rm H\,I}) = 10^{12-15}\,{\rm cm}^{-2}$ (right panel of Fig. 2).

The large N(H I) in the neutral medium produces pronounced damping wings in the QSO spectrum. These absorbers are commonly referred to as damped Lyα absorbers (DLAs). An example is shown in the second panel from the top in Fig. 1. In this particular case, a simultaneous fit to the QSO continuum and the damping wings (red curve in the second panel from the top) yields a best-fit $\log N({\rm H\,I}) = 21.45 \pm 0.05$ for the DLA. At intermediate N(H I), LLS and pLLS are identified based on the apparent flux discontinuities in QSO spectra (top panel). A significant fraction of these strong Lyα absorbers have been enriched with heavy elements which produce additional absorption features due to heavy ions in the QSO spectra. The most prominent features include the O VI $\lambda\lambda$ 1031, 1037 doublet transitions which occur in the Lyα forest, and the C IV $\lambda\lambda$ 1548, 1550 and Mg II $\lambda\lambda$ 2796, 2803 doublets, plus a series of low-ionization transitions such as C II, Si II, and Fe II. Together, these ionic transitions constrain the ionization state and chemical compositions of the gas (e.g., Chen and Prochaska 2000; Werk et al 2014).

Combining galaxy surveys with absorption-line observations of gas around galaxies enables comprehensive studies of baryon cycles between star-forming regions and low-density gas over cosmic time. At low redshifts, $z \lesssim 0.2$, deep 21 cm and CO surveys have revealed exquisite details of the cold gas content ($T \lesssim 1000$ K) in nearby galaxies, providing both new clues and puzzles in the overall understanding of galaxy formation and evolution. These include extended H I disks around blue star-forming galaxies with the H I extent $\approx 2\times$ what is found for the stellar disk (e.g., Swaters et al 2002; Walter et al 2008; Leroy et al 2008), extended H I and molecular gas in early-type galaxies (e.g., Oosterloo et al 2010; Serra et al 2012) with predominantly old stellar populations and little or no on-going star formation (Salim and Rich 2010), and widespread H I streams connecting regular-looking galaxies in group environments (e.g., Verdes-Montenegro et al 2001; Chynoweth et al 2008).

Figure 2 (left panel) showcases an example of a deep 21 cm image of the M81 group, a poor group of dynamical mass $M_{\rm dyn} \sim 10^{12}\,M_{\odot}$ (Karachentsev and Kashibadze 2006). Prominent group members include the grand-design spiral galaxy M81 at the centre, the proto-starburst galaxy M82, and several other lower-mass satellites (Burbidge and Burbidge 1961). The 21 cm image displays a diverse array of gaseous structures in the M81 group, from extended rotating disks, warps, high velocity clouds (HVCs), tidal tails and filaments, to bridges connecting what appear to be optically isolated galaxies. High column density gaseous streams of

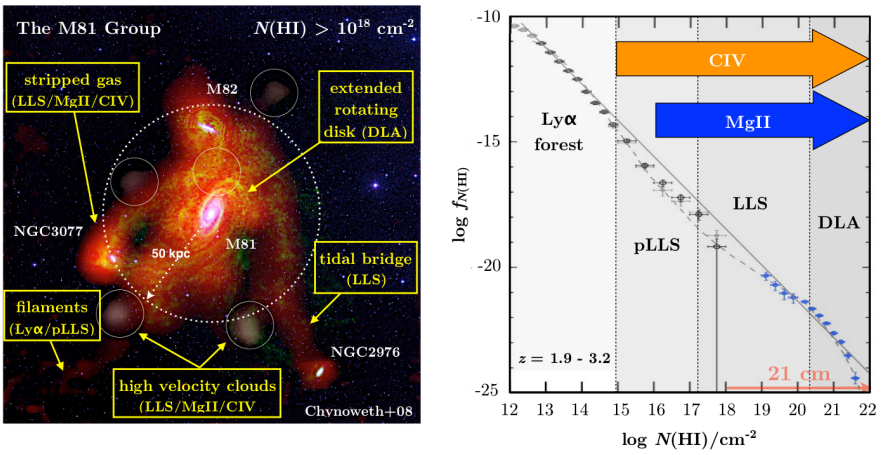

Fig. 2 Mapping galaxy outskirts in 21 cm and in QSO absorption-line systems. *Left*: Deep 21 cm image of the M81 group, revealing a complex interface between stars and gas in the group. The observed neutral hydrogen column densities range from $N(\mathrm{H\,I}) \sim 10^{18}\,\mathrm{cm}^{-2}$ in the filamentary structures to $N(\mathrm{H\,I}) > 10^{21}\,\mathrm{cm}^{-2}$ in the star-forming disks of group members (Yun et al 1994; Chynoweth et al 2008). The 21 cm image reveals a diverse array of gaseous structures in this galaxy group, but these observations become extremely challenging beyond redshift $z \approx 0.2$ (e.g., Verheijen et al 2007; Fernández et al 2013). *Right*: The H I column density distribution function of Lyα absorbers, $f_{N(\mathrm{H\,I})}$, uncovered at $z = 1.9 - 3.2$ along sightlines toward random background QSOs (adapted from Kim et al 2013). Quasar absorbers in different categories are mapped onto different H I structures both seen and missed in the 21 cm image in the left panel. Specifically, DLAs probe the star-forming ISM and extended rotating disks, LLS probe the gaseous streams connecting different group members as well as stripped gas and high velocity clouds around galaxies, and pLLS and strong Lyα absorbers trace ionized gas that is not observed in 21 cm signals. Among the quasar absorbers, C IV absorption transitions are commonly observed in strong Lyα absorbers of $N(\mathrm{H\,I}) \gtrsim 10^{15}\,\mathrm{cm}^{-2}$ (see e.g., Kim et al 2013; D'Odorico et al 2016), and Mg II absorption transitions are seen in most high-$N(\mathrm{H\,I})$ absorbers of $N(\mathrm{H\,I}) \gtrsim 10^{16}\,\mathrm{cm}^{-2}$ (see e.g., Rigby et al 2002). These metal-line absorbers trace chemically enriched gas in and around galaxies

$N(\mathrm{H\,I}) \gtrsim 10^{18}\,\mathrm{cm}^{-2}$ are seen extending beyond 50 kpc in projected distance from M81, despite the isolated appearances of M81 and other group members in optical images. These spatially resolved imaging observations of different gaseous components serve as important tests for theoretical models of galaxy formation and evolution (e.g., Agertz et al 2009; Marasco et al 2016). However, 21 cm imaging observations are insensitive to warm ionized gas of $T \sim 10^4$ K and become extremely challenging for galaxies beyond redshift $z = 0.2$ (e.g., Verheijen et al 2007; Fernández et al 2013).

QSO absorption spectroscopy extends 21 cm maps of gaseous structures around galaxies to both lower gas column density and higher redshifts. Based on the characteristic $N(\mathrm{H\,I})$, direct analogues can be drawn between different types of QSO absorbers and different gaseous components seen in deep 21 cm images of nearby galaxies. For example, DLAs probe the neutral gas in the interstellar medium

(ISM) and extended rotating disks, LLS probe optically thick gaseous streams and high velocity clouds in galaxy haloes, and pLLS and strong Lyα absorbers of $N(\mathrm{H\,I}) \approx 10^{14-17}\,\mathrm{cm}^{-2}$ trace ionized halo gas and starburst outflows (e.g., supergalactic winds in M 82 Lehnert et al 1999) that cannot be reached with 21 cm observations.

The right panel of Fig. 2 displays the H I column density distribution function, $f_{N(\mathrm{H\,I})}$, for all Lyα absorbers uncovered at $z = 1.9 - 3.2$ along random QSO sightlines (Kim et al 2013). $f_{N(\mathrm{H\,I})}$, defined as the number of Lyα absorbers per unit absorption pathlength per unit H I column density interval, is a key statistical measure of the Lyα absorber population. It represents a cross-section weighted surface density profile of hydrogen gas in a cosmological volume. With sufficiently high spectral resolution and high signal-to-noise, $S/N \gtrsim 30$, QSO absorption spectra probe tenuous gas with $N(\mathrm{H\,I})$ as low as $N(\mathrm{H\,I}) \sim 10^{12}\,\mathrm{cm}^{-2}$. The steeply declining $f_{N(\mathrm{H\,I})}$ with increasing $N(\mathrm{H\,I})$ shows that the occurrence (or areal coverage) of pLLS and strong Lyα absorbers of $N(\mathrm{H\,I}) \approx 10^{14-17}\,\mathrm{cm}^{-2}$ is ≈ 10 times higher than that of optically thick LLS along a random sightline and ≈ 100 times higher than the incidence of DLAs. Such a differential frequency distribution is qualitatively consistent with the spatial distribution of H I gas recorded in local 21 cm surveys (e.g., Fig. 2, left panel), where gaseous disks with $N(\mathrm{H\,I})$ comparable to DLAs cover a much smaller area on the sky than streams and HVCs with $N(\mathrm{H\,I})$ comparable to LLS. If a substantial fraction of optically thin absorbers originate in galaxy haloes, then their higher incidence implies a gaseous halo of size at least three times what is seen in deep 21 cm images.

In addition, many of these strong Lyα absorbers exhibit associated transitions due to heavy ions. In particular, C IV absorption transitions are commonly observed in strong Lyα absorbers of $N(\mathrm{H\,I}) \gtrsim 10^{15}\,\mathrm{cm}^{-2}$ (see, e.g., Kim et al 2013; D'Odorico et al 2016), and Mg II absorption transitions are seen in most high-$N(\mathrm{H\,I})$ absorbers of $N(\mathrm{H\,I}) \gtrsim 10^{16}$ cm^{-2} (e.g., Rigby et al 2002). While Mg II absorbers are understood to originate in photo-ionized gas of temperature $T \sim 10^4$ K (e.g., Bergeron and Stasińska 1986), C IV absorbers are more commonly seen in complex, multi-phase media (e.g., Rauch et al 1996; Boksenberg and Sargent 2015). These metal-line absorbers therefore offer additional probes of chemically enriched gas in and around galaxies.

This Chapter presents a brief review of the current state of knowledge on the outskirts of distant galaxies from absorption-line studies. The review will first focus on the properties of the neutral gas reservoir probed by DLAs, and then outline the insights into star formation and chemical enrichment in the outskirts of distant galaxies from searches of DLA galaxies. A comprehensive review of DLAs is already available in Wolfe et al (2005). Therefore, the emphasis here focusses on new findings over the past decade. Finally, a brief discussion will be presented on the empirical properties and physical understandings of the ionized circumgalactic gas as probed by strong Lyα and various metal-line absorbers.

2 Tracking the Neutral Gas Reservoir Over Cosmic Time

DLAs are historically defined as Lyα absorbers with neutral hydrogen column densities exceeding $N(\mathrm{H\,I}) = 2\times10^{20}\,\mathrm{cm}^{-2}$ (Wolfe et al 2005), corresponding to a surface mass density limit of $\Sigma_{\rm atomic} \approx 2 M_\odot\,\mathrm{pc}^{-2}$ for atomic gas (including helium). The large gas surface mass densities revealed in high-redshift DLAs are comparable to what is seen in 21 cm observations of nearby star-forming galaxies (e.g., Walter et al 2008; Leroy et al 2008), making DLAs a promising signpost of young galaxies in the distant Universe (Wolfe et al 1986). In addition, the $N(\mathrm{H\,I})$ threshold ensures that the gas is neutral under the metagalactic ionizing radiation field (e.g., Viegas 1995; Prochaska and Wolfe 1996; Prochaska et al 2002). Neutral gas provides the seeds necessary for sustaining star formation. Therefore, observations of DLAs not only help establish a census of the cosmic evolution of the neutral gas reservoir (e.g., Neeleman et al 2016a), but also offer a unique window into star formation physics in distant galaxies (e.g., Lanzetta et al 2002; Wolfe and Chen 2006).

While the utility of DLAs for probing the young Universe is clear, these objects are relatively rare (see the right panel of Fig. 2) and establishing a statistically representative sample of these rare systems requires a large sample of QSO spectra. Over the last decade, significant progress has been made in characterizing the DLA population at $z\gtrsim2$, owing to the rapidly growing spectroscopic sample of high-redshift QSOs from the Sloan Digital Sky Survey (SDSS; York et al 2000). The blue points in the right panel of Fig. 2 are based on ~1000 DLAs and ~500 strong LLS identified at $z\approx2-5$ in an initial SDSS DLA sample (Noterdaeme et al 2009). The sample of known DLAs at $z\gtrsim2$ has continued to grow, reaching $\sim10,000$ DLAs found in the SDSS spectroscopic QSO sample (e.g., Noterdaeme et al 2012).

The large number of known DLAs has led to an accurate characterization of the neutral gas reservoir at high redshifts. Figure 3a displays the observed $N(\mathrm{H\,I})$ distribution function, $f_{\rm DLA}$, based on ~7000 DLAs identified at $z\approx2-5$ (Noterdaeme et al 2012). The plot shows that $f_{\rm DLA}$ is well represented by a Schechter function (Schechter 1976) at $\log N(\mathrm{H\,I})\lesssim22$ following

$$f_{\rm DLA}\equiv f_{N(\mathrm{H\,I})}(\log N(\mathrm{H\,I})\geq20.3)\propto\left[\frac{N(\mathrm{H\,I})}{N_*(\mathrm{H\,I})}\right]^{\alpha}\exp[-N(\mathrm{H\,I})/N_*(\mathrm{H\,I})],\qquad(1)$$

with a shallow power-law index of $\alpha\approx-1.3$ below the characteristic H I column density $\log N_*(\mathrm{H\,I})\approx21.3$ and a steep exponential decline at larger $N(\mathrm{H\,I})$ (Noterdaeme et al 2009, 2012). At $\log N(\mathrm{H\,I})>22$, the observations clearly deviate from the best-fit Schechter function. However, DLAs are also exceedingly rare in this high-$N(\mathrm{H\,I})$ regime. Only eight such strong DLAs have been found in this large DLA sample (Noterdaeme et al 2012), making measurements of $f_{\rm DLA}$ in the two highest-$N(\mathrm{H\,I})$ bins very uncertain. In comparison to $f_{N(\mathrm{H\,I})}$ established from 21 cm maps of nearby galaxies (Zwaan et al 2005), the amplitude of $f_{\rm DLA}$ at $z\gtrsim2$ is $\approx2\times$ higher than $f_{N(\mathrm{H\,I})}$ at $z\approx0$ but the overall shapes are remarkably similar at both low- and high-$N(\mathrm{H\,I})$ regimes (Fig. 3a; see also Sánchez-Ramírez et al 2016; Rafelski et al 2016).

At $\log N(\mathrm{H\,I}) > 21$, numerical simulations have shown that the predicted shape in f_{DLA} is sensitive to the detailed ISM physics, including the formation of molecules (H_2) and different feedback processes (e.g., Altay et al 2011, 2013; Bird et al 2014). Comparison of the observed and predicted f_{DLA} therefore provides an independent and critical test for the prescriptions of these physical processes in cosmological simulations. However, the constant exponentially declining trend at $N(\mathrm{H\,I}) \gtrsim 2\times10^{21}\,\mathrm{cm}^{-2}$ between low-redshift H I galaxies and high-redshift DLAs presents a puzzle.

At $z = 0$, the rapidly declining $f_{N(\mathrm{H\,I})}$ at $N(\mathrm{H\,I}) \gtrsim N_*(\mathrm{H\,I})$ has been interpreted as due to the conversion of atomic gas to molecular gas (Zwaan and Prochaska 2006; Braun 2012). As illustrated at the end of this Section and in Fig. 3d, the column density threshold beyond which the gas transitions from H I to H_2 depends strongly on the gas metallicity, and the mean metallicity observed in the atomic gas decreases steadily from $z \approx 0$ to $z > 4$ (Fig. 3c). Therefore, the conversion to molecules in high-redshift DLAs is expected to occur at higher $N(\mathrm{H\,I})$, resulting in a higher $N_*(\mathrm{H\,I})$ with increasing redshift. However, this is not observed (e.g., Prochaska and Wolfe 2009; Sánchez-Ramírez et al 2016; Rafelski et al 2016; Fig. 3a). Based on spatially resolved 21 cm maps of nearby galaxies with ISM metallicity spanning over a decade, it has been shown that $f_{N(\mathrm{H\,I})}$ established individually for these galaxies does not vary significantly with their ISM metallicity (Erkal et al 2012). Together, these findings demonstrate that the exponential decline of f_{DLA} at $N(\mathrm{H\,I}) \gtrsim N_*(\mathrm{H\,I})$ is not due to conversion of H I to H_2, but the physical origin remains unknown.

Nevertheless, the observed f_{DLA} immediately leads to two important statistical quantities: (1) the number density of DLAs per unit survey pathlength, obtained by integrating f_{DLA} over all $N(\mathrm{H\,I})$ greater than $N_0 = 2\times10^{20}\,\mathrm{cm}^{-2}$ and (2) the cosmic neutral gas mass density, contained in DLAs, Ω_{atomic}, which is the $N(\mathrm{H\,I})$-weighted integral of f_{DLA} following

$$\Omega_{\mathrm{atomic}} \equiv \rho_{\mathrm{gas}}/\rho_{\mathrm{crit}} = \int_{N_0}^{\infty} (\mu\, H_0/c/\rho_{\mathrm{crit}})\, N(\mathrm{H\,I})\, f_{\mathrm{DLA}}\, dN(\mathrm{H\,I}), \qquad (2)$$

where $\mu = 1.3$ is the mean atomic weight of the gas particles (accounting for the presence of helium), H_0 is the Hubble constant, c is the speed of light, and ρ_{crit} is the critical density of the Universe (e.g., Lanzetta et al 1991; Wolfe et al 1995). The shallow power-law index α in the best-fit f_{DLA}, together with a steep exponential decline at high $N(\mathrm{H\,I})$ from the Schechter function in Eq. (1), indicates that while DLAs of $N(\mathrm{H\,I}) < N_*(\mathrm{H\,I})$ dominate the neutral gas cross-section (and therefore the number density), strong DLAs of $N(\mathrm{H\,I}) \sim N_*(\mathrm{H\,I})$ contribute predominantly to the neutral mass density in the Universe (e.g., Zwaan et al 2005). A detailed examination of the differential Ω_{atomic} distribution as a function of $N(\mathrm{H\,I})$ indeed confirms that the bulk of neutral gas is contained in DLAs of $N(\mathrm{H\,I}) \approx 2\times10^{21}\,\mathrm{cm}^{-2}$ (e.g., Noterdaeme et al 2012).

The cosmic evolution of ρ_{gas} observed in DLAs, from Eq. (2), is shown in black points in Fig. 3b. Only measurements based on blind DLA surveys are presented

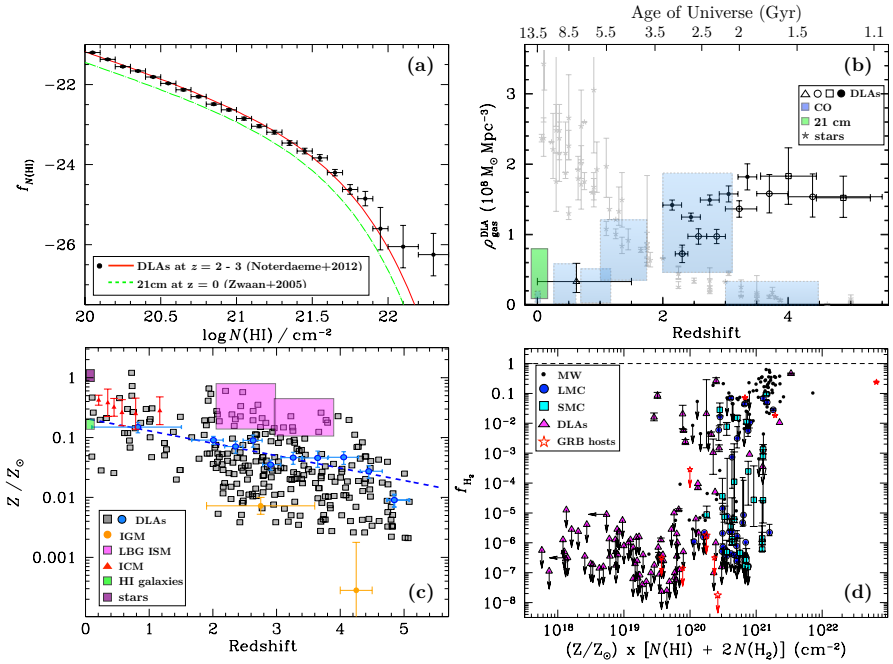

Fig. 3 Summary of known DLA properties: (*a*) evolving neutral hydrogen column density distribution functions, $f_{N(\mathrm{H\,I})}$ from DLAs at $z = 2-3$ (Noterdaeme et al 2012) to H I galaxies at $z \approx 0$ (Zwaan et al 2005); (*b*) declining cosmic neutral gas mass density with increasing Universe age (or decreasing redshift) from observations of DLAs (solid points from Noterdaeme et al 2012, open circles from Prochaska and Wolfe 2009, open squares from Crighton et al 2015, and open triangle from Neeleman et al 2016a) following Eq. (2), local H I galaxies (green shaded box, a compilation from Neeleman et al 2016a), and molecular gas (blue shaded boxes, Decarli et al 2016), in comparison to increasing cosmic stellar mass density in galaxies with increasing Universe age (grey asterisks, a compilation from Madau and Dickinson 2014); (*c*) gas-phase metallicity (Z) relative to Solar ($Z_\odot$) as a function of redshift in DLAs (grey squares for individual absorbers and blue points for $N(\mathrm{H\,I})$-weighted mean from Marc Rafelski, Rafelski et al 2012, 2014), IGM at $z \gtrsim 2$ (orange circles, Aguirre et al 2008; Simcoe 2011), ISM of starburst galaxies at $z \approx 2-4$ (light magenta boxes, Pettini et al 2001; Pettini 2004; Erb et al 2006a; Maiolino et al 2008; Mannucci et al 2009), intracluster medium in X-ray luminous galaxy clusters at $z \lesssim 1$ (red triangles, Balestra et al 2007), H I-selected galaxies (green box, Zwaan et al 2005), and stars at $z = 0$ (dark purple box, Gallazzi et al 2008); and (*d*) molecular gas fraction, $f_{\mathrm{H_2}}$ versus total surface density of neutral gas scaled by gas metallicity for high-redshift DLAs in triangles (Noterdaeme et al 2008, 2016), γ-ray burst host ISM in star symbols (e.g., Noterdaeme et al 2015), and local ISM in the Milky Way (Wolfire et al 2008) and Large and Small Magellanic Clouds (Tumlinson et al 2002) in dots, blue circles, and cyan squares, respectively

in the plot[1]. These include an early sample of ≈ 700 DLAs at $z = 2.5-5$ in the SDSS Data Release (DR) 5 (open circles; Prochaska and Wolfe 2009), an expanded sample of ≈ 7000 DLAs in the SDSS DR12 (solid points; Noterdaeme et al 2012), an expanded high-redshift sample of DLAs at $z = 4-5$ (open squares; Crighton et al 2015), and a sample of ≈ 14 DLAs at $z \lesssim 1.6$ from an exhaustive search in the *Hubble Space Telescope* (*HST*) UV spectroscopic archive (open triangle; Neeleman et al 2016a).

A range of mean H I mass density at $z \approx 0$ has been reported from different 21 cm surveys (see Neeleman et al 2016a for a recent compilation). These measurements are included in the green box in Fig. 3b. Despite a relatively large scatter between different 21 cm surveys and between DLA surveys, a steady decline in $\Omega_{\rm atomic}$ is observed from $z \approx 4$ to $z \approx 0$. For comparison, the cosmic evolution of the molecular gas mass density obtained from a recent blind CO survey (Decarli et al 2016) is also included as blue-shaded boxes in Fig. 3b, along with the cosmic evolution of stellar mass density measured in different galaxy surveys, shown in grey asterisks (data from Madau and Dickinson 2014). Figure 3b shows that the decline in the neutral gas mass density with decreasing redshift is coupled with an increase in the mean stellar mass density in galaxies, which is qualitatively consistent with the expectation that neutral gas is being consumed to form stars. However, it is also clear that atomic gas alone is insufficient to explain the observed order-of-magnitude gain in the total stellar mass density from $z \approx 3$ to $z \approx 0$, which implies the need for replenishing the neutral gas reservoir with accretion from the intergalactic medium (IGM) (e.g., Kereš et al 2009; Prochaska and Wolfe 2009). At the same time, new blind CO surveys have shown that molecular gas contributes roughly an equal amount of neutral gas mass density as atomic gas observed in DLAs at $z \lesssim 3$ (e.g., Walter et al 2014; Decarli et al 2016), although the uncertainties are still very large. Together with the knowledge of an extremely low molecular gas fraction in DLAs (see the discussion on the next page and Fig. 3d), these new CO surveys indicate that previous estimates of the total neutral gas mass density based on DLAs alone have been underestimated by as much as a factor of two. An expanded blind CO survey over a cosmological volume is needed to reduce the uncertainties in the observed molecular gas mass densities at different redshifts, which will cast new insights into the connections between star formation, the neutral gas reservoir, and the ionized IGM over cosmic time.

Observations of the chemical compositions of DLAs provide additional clues to the connection between the neutral gas probed by DLAs and star formation (e.g.,

[1] At $z \lesssim 1.6$, DLA surveys require QSO spectroscopy carried out in space and have been limited to the number of UV-bright QSOs available for absorption line searches. Consequently, the number of known DLAs from blind surveys is small, ≈ 15 (see Neeleman et al 2016a for a compilation). To increase substantially the sample of known DLAs at low redshifts, Rao & Turnshek (Rao et al 2006) devised a clever space programme to search for new DLAs in known Mg II absorbers. Their strategy yielded a substantial gain, tripling the total sample size of $z \lesssim 1.6$ DLAs. However, the Mg II-selected DLA sample also includes a survey bias that is not well understood. It has been shown that excluding Mg II-selected DLAs reduces the inferred $\Omega_{\rm atomic}$ by more than a factor of four (e.g., Neeleman et al 2016a). For consistency, only measurements of $\Omega_{\rm atomic}$ based on blind DLA surveys are included in the plot.

Pettini 2004). In particular, because the gas is predominantly neutral, the dominant ionization for most heavy elements (such as Mg, Si, S, Fe, Zn, etc.) are in the singly ionized state and therefore the observed abundances of these low-ionization species place direct and accurate constraints on the elemental abundances of the gas (e.g., Viegas 1995; Prochaska and Wolfe 1996; Vladilo et al 2001; Prochaska et al 2002). Additional constraints on the dust content and on the sources that drive the chemical enrichment history in DLAs can be obtained by comparing the relative abundances of different elements. Specifically, comparing the relative abundances between refractory (such as Cr and Fe) and non-refractory elements (such as S and Zn) indicates the presence of dust in the neutral gas, the amount of which increases with metallicity (e.g., Meyer et al 1989; Pettini et al 1990; Savage and Sembach 1996; Wolfe et al 2005). The relative abundances of α- to Fe-peak elements determine whether core-collapse supernovae (SNe) or SNe Ia dominate the chemical enrichment history, and DLAs typically exhibit an α-element enhanced abundance pattern (e.g., Lu et al 1996; Pettini et al 1999; Prochaska and Wolfe 1999).

Figure 3c presents a summary of gas metallity (Z) relative to Solar ($Z_\odot$) measured for >250 DLAs at $z \lesssim 5$ (grey squares from Rafelski et al 2012, 2014). The cosmic mean gas metallicity in DLAs as a function of redshift can be determined based on a $N(\mathrm{H\,I})$-weighted average over an ensemble of DLAs in each redshift bin (blue points), which is found to increase steadily with decreasing redshift following a best-fit mean relation of $\langle Z/Z_\odot \rangle = [-0.20 \pm 0.03]\,z - [0.68 \pm 0.09]$ (dashed blue line, Rafelski et al 2014). For comparison, the figure also includes measurements for stars (dark purple box, Gallazzi et al 2008) and H I-selected galaxies (green box, Zwaan et al 2005) at $z = 0$, iron abundances in the intracluster medium in X-ray luminous galaxy clusters at $z \lesssim 1$ (red triangles, Balestra et al 2007), ISM of starburst galaxies (light magenta boxes) at $z \approx 2-3$ (Pettini et al 2001; Pettini 2004; Erb et al 2006a) and at $z = 3-4$ (Maiolino et al 2008; Mannucci et al 2009), and IGM at $z \gtrsim 2$ (orange circles, Aguirre et al 2008; Simcoe 2011).

It is immediately clear from Fig. 3c that there exists a large scatter in the observed metallicity in DLAs at all redshifts. In addition, while the cosmic mean metallicity in DLAs is significantly higher than what is observed in the low-density IGM, it remains lower than what is observed in the star-forming ISM at $z = 2-4$ and a factor of ≈ 5 below the mean values observed in stars at $z = 0$. The chemical enrichment level in DLAs is also lower than the iron abundances seen in the intracluster medium at intermediate redshifts. The observed low metallicity relative to the measurements in and around known luminous galaxies raised the question of whether or not the DLAs probe preferentially low-metallicity, gas-rich galaxies and are not representative of more luminous, metal-rich galaxies found in large-scale surveys (e.g., Pettini 2004).

The large scatter in the observed metallicity in DLAs is found to be explained by a combination of two factors (Chen et al 2005): (i) the mass-metallicity (or luminosity-metallicity) relation in which more massive galaxies on average exhibit higher global ISM metallicities (e.g., Tremonti et al 2004; Erb et al 2006a; Neeleman et al 2013; Christensen et al 2014) and (ii) metallicity gradients commonly seen in star-forming disks with lower metallicities at larger distances (e.g., Zaritsky et al

1994; van Zee et al 1998; Sánchez et al 2014; Wuyts et al 2016). If DLAs sample a representative galaxy population including both low-mass and massive galaxies and probe both inner and outer disks of these galaxies, then a large metallicity spread is expected.

The observed low metallicity in DLAs, relative to star-forming ISM, is also understood as due to a combination of DLAs being a gas cross-section selected sample and the presence of metallicity gradients in disk galaxies (Chen et al 2005). A cross-section selected sample contains a higher fraction of absorbers originating in galaxy outskirts than in the inner regions, and the presence of metallicity gradients indicates that galaxy outskirts have lower metallicities than what is observed in inner disks (see Sect. 3 and Fig. 4 below for more details). Indeed, including both factors, a gas cross-section weighting scheme and a metallicity gradient, for local H I galaxies resulted in a mean metallicity comparable to what is observed in DLAs (green box in Fig. 3c; Zwaan et al 2005).

While DLAs exhibit a moderate level of chemical enrichment, searches for molecular gas in DLAs have yielded only a few detections (e.g., Noterdaeme et al 2008; Jorgenson et al 2014; Noterdaeme et al 2016). Figure 3d displays the observed molecular gas fraction, which is defined as $f_{\rm H_2} \equiv 2N({\rm H_2})/[N({\rm H\,I}) + 2N({\rm H_2})]$, versus metallicity-scaled total hydrogen column density for ≈ 100 DLAs at $z \approx 2-4$ (triangles). The DLAs span roughly two decades in $N({\rm H\,I})$ from $N({\rm H\,I}) \approx 2 \times 10^{20}\,{\rm cm^{-2}}$ to $N({\rm H\,I}) \approx 2.5 \times 10^{22}\,{\rm cm^{-2}}$. Strong limits have been placed for $f_{\rm H_2}$ for the majority of DLAs at $f_{\rm H_2} \lesssim 10^{-5}$ with only $\approx 10\%$ displaying the presence of H_2 and two having $f_{\rm H_2} > 0.1$. In contrast, the ISM of the Milky Way (MW), at comparable $N({\rm H\,I})$, displays a much higher $f_{\rm H_2}$ than the DLAs at high redshifts.

The formation of molecules is understood to depend on two competing factors: (i) the ISM radiation field which photo-dissociates molecules and (ii) dust which facilitates molecule formation (e.g., Elmegreen 1993; Cazaux and Spaans 2004). Dust is considered a more dominant factor because of its dual roles in both forming molecules and shielding them from the ISM radiation field. In star-forming galaxies, the dust-to-gas mass ratio is observed to correlate strongly with ISM gas-phase metallicity (e.g., Leroy et al 2011; Rémy-Ruyer et al 2014). It is therefore expected that the observed molecular gas fraction should correlate with gas metallicity (e.g., Elmegreen 1989; Krumholz et al 2009; Gnedin et al 2009).

In the MW ISM with metallicity roughly Solar, $Z \approx Z_\odot$, the molecular gas fraction is observed to increase sharply from $f_{\rm H_2} < 10^{-4}$ to $f_{\rm H_2} \gtrsim 0.1$ at $N({\rm H\,I}) \approx 2 \times 10^{20}\,{\rm cm^{-2}}$ (see Wolfire et al 2008). The sharp transition from atomic to molecular is also observed in the ISM of the Large and Small Magellanic Clouds (LMC and SMC), but occurs at higher gas column densities of $N({\rm H\,I}) \approx 10^{21}\,{\rm cm^{-2}}$ for the LMC and $N({\rm H\,I}) \approx 3 \times 10^{21}\,{\rm cm^{-2}}$ for the SMC (see Tumlinson et al 2002). The ISM metallicities of LMC and SMC are $Z \approx 0.5\,Z_\odot$ and $Z \approx 0.15\,Z_\odot$, respectively. These observations therefore support a simple metallicity-dependent transitional gas column density illustrated in Fig. 3d. Following the metallicity-scaling relation, it is clear that despite a high $N({\rm H\,I})$, most DLAs do not have sufficiently high metallicity (and therefore dust content) to facilitate the formation of molecules (Gnedin and Kravtsov 2010; Gnedin and Draine 2014; Noterdaeme et al 2015). This finding also

applies to γ-ray burst (GRB) host galaxies (star symbols in Fig. 3d). With few exceptions (Prochaska et al 2009; Krühler et al 2013; Friis et al 2015, the ISM in most GRB hosts displays a combination of very high $N(\mathrm{H\,I})$ and low $f_{\mathrm{H_2}}$ (e.g., Tumlinson et al 2007; Ledoux et al 2009). The observed absence of H_2 in DLAs, together with a large molecular mass density revealed in blind CO surveys (e.g., Walter et al 2014; Decarli et al 2016), shows that a complete census for the cosmic evolution of the neutral gas reservoir requires complementary surveys of molecular gas over a broad redshift range. In addition, as described in Sect. 4 below, the observed low molecular gas content also has important implications for star formation properties in metal-deficient, high neutral gas surface density environments.

3 Probing the Neutral Gas Phase in Galaxy Outskirts

Considerable details have been learned about the physical properties and chemical enrichment in neutral atomic gas from DLA studies. To apply the knowledge of DLAs for a better understanding of distant galaxies, it is necessary to first identify DLA galaxies and compare them with the general galaxy population. Searches for DLA galaxies are challenging, because distant galaxies are faint and because the relatively small extent of high-$N(\mathrm{H\,I})$ gas around galaxies places the absorbing galaxies at small angular distances from the bright background QSOs. Based on a well-defined H I size-mass relation observed in local H I galaxies (e.g., Broeils and Rhee 1997; Verheijen and Sancisi 2001; Swaters et al 2002), the characteristic projected separation (accounting for weighting by cross section) between a DLA and an L_* absorbing galaxy is ≈ 16 kpc and smaller for lower-mass galaxies. At $z = 1-2$, a projected distance of 16 kpc corresponds to an angular separation of $\lesssim 2''$, and greater at lower and higher redshifts.

While fewer DLAs are known at $z \lesssim 1$ (see Sect.2), a large number (≈ 40) of these low-redshift DLAs have their galaxy counterparts (or candidates) found based on a combination of photometric and spectroscopic techniques (e.g., Chen and Lanzetta 2003; Rao et al 2003, 2011; Péroux et al 2016). It has been shown based on this low-redshift DLA galaxy sample that DLAs probe a representative galaxy population in luminosity and colour. DLA galaxies are consistent with an H I cross-section selected sample with a large fraction of DLAs found at projected distance $d \gtrsim 10$ kpc from the absorbing galaxies (e.g., Chen and Lanzetta 2003; Rao et al 2011). In addition to regular disk galaxies, two DLAs have been found in a group environment (e.g., Bergeron and Boissé 1991; Chen and Lanzetta 2003; Kacprzak et al 2010; Péroux et al 2011), suggesting that stripped gas from galaxy interactions could also contribute to the incidence of DLAs. The low-redshift DLA sample is expected to continue to grow dramatically with new discoveries from the SDSS (e.g., Straka et al 2015). In contrast, the search for DLA galaxies at $z > 2$ has been less successful despite extensive efforts (e.g., Warren et al 2001; Møller et al 2002; Péroux et al 2012; Fumagalli et al 2015). To date, only ≈ 12 DLA galaxies have been found at $z > 2$ (Krogager et al 2012; Fumagalli et al 2015).

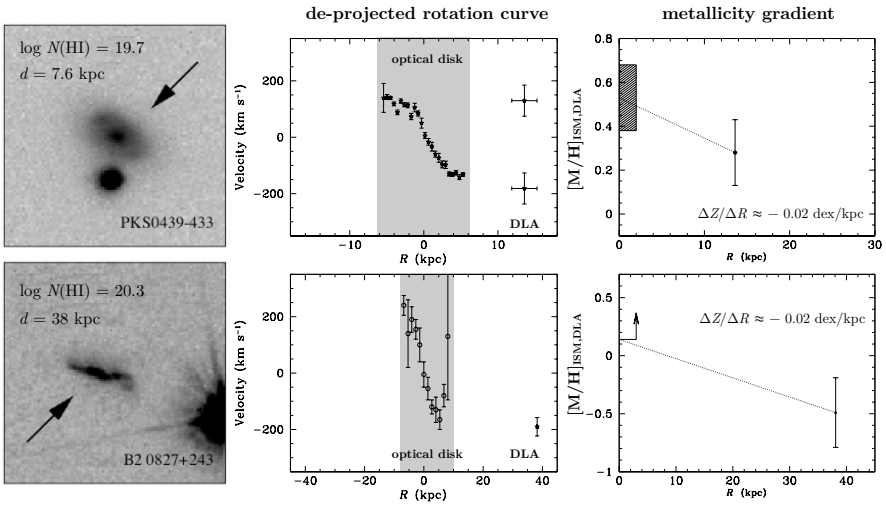

Fig. 4 Neutral gas kinematics and metallicity revealed by the presence of a DLA in the outskirts of two L_* galaxies (adapted from Chen et al 2005). The *top* row presents a DLA found at $d = 7.6$ kpc from a disk galaxy at $z = 0.101$, which also exhibits widespread CO emission in the disk (Neeleman et al 2016b). The *bottom* row presents a DLA at $d = 38$ kpc from an edge-on disk at $z = 0.525$. Deep r-band images of the galaxies are presented in the *left* panels, which display spatially resolved disk morphologies and enable accurate measurements of the inclination and orientation of the optical disk. The *middle* panels present the optical rotation curves deprojected along the disk plane (points in shaded area) based on the inclination angle determined from the optical image of each galaxy (Eq. 3 & 4). If the DLAs occur in extended disks, the corresponding galactocentric distances of the two galaxies from Eq. (3) are $R = 13.6$ kpc (top) and $R = 38$ kpc (bottom). The DLA in the *top* panel is resolved into two components of comparable ionic column densities (Som et al 2015) but an order of magnitude difference in $N(\mathrm{H_2})$ (Muzahid et al 2015). The component with a lower $N(\mathrm{H_2})$ appears to be co-rotating with the optical disk (lower DLA data point), while the component with stronger $N(\mathrm{H_2})$ appears to be counter-rotating, possibly due to a satellite (upper DLA data point). The DLA in the *bottom* panel displays simpler gas kinematics consistent with an extended rotating disk out to ≈ 40 kpc. The *right* panels present the metallicity gradient observed in the gaseous disks based on comparisons of ISM gas-phase metallicity and metallicity of the DLA beyond the optical disks. In both cases, the gas metallicity declines with increasing radius according to $\Delta Z/\Delta R = -0.02$ dex kpc^{-1}

In addition to a general characterization of the DLA galaxy population, individual DLA and galaxy pairs provide a unique opportunity to probe neutral gas in the outskirts of distant galaxies. Figure 4 shows two examples of constraining the kinematics and chemical enrichment in the outskirts of neutral disks from combining resolved optical imaging and spectroscopy of the galaxy with an absorption-line analysis of the DLA. In the first example (top row), a DLA of $\log N(\mathrm{H\,I}) = 19.7$ is found at $d = 7.6$ kpc from an L_* galaxy at $z = 0.101$, which also exhibits widespread CO emission in the disk (Neeleman et al 2016b). The galaxy disk is resolved in the ground-based r-band image (upper-left panel), which enables accurate measurements of the disk inclination and orientation (Chen et al 2005). While the observed

$N(\mathrm{H\,I})$ falls below the nominal threshold of a DLA, the gas is found to be largely neutral (e.g., Chen et al 2005; Som et al 2015). In addition, abundant H_2 is detected in the absorbing gas (Muzahid et al 2015). Optical spectra of the galaxy clearly indicate a strong velocity shear along the disk, suggesting an organized rotation motion (Chen et al 2005) which is confirmed by recent CO observations (Neeleman et al 2016b). At the same time, the DLA is resolved into two components of comparable ionic column densities (Som et al 2015) but an order of magnitude difference in $N(\mathrm{H_2})$ (Muzahid et al 2015). A rotation curve of the gaseous disk extending beyond 10 kpc (top-centre panel) can be established based on the observed velocity shear ($v_{\rm obs}$) and deprojection onto the disk plane following

$$\frac{R}{d} = \sqrt{1+\sin^2(\phi)\tan^2(i)} \tag{3}$$

and

$$v = \frac{v_{\rm obs}}{\cos(\phi)\sin(i)}\sqrt{1+\sin^2(\phi)\tan^2(i)}, \tag{4}$$

where R is the galactocentric radius along the disk, v is the deprojected rotation velocity, i is the inclination angle of the disk, and ϕ is the azimuthal angle from the major axis of the disk where the DLA is detected (Chen et al 2005, see also Steidel et al 2002 for an alternative formalism). For the two absorbing components in this DLA, it is found that the component with a lower $N(\mathrm{H_2})$ appears to be co-rotating with the optical disk (lower DLA data point), while the component with stronger $N(\mathrm{H_2})$ appears to be counter-rotating, possibly due to a satellite (upper DLA data point). Comparing the ISM gas-phase metallicity and the metallicity of the DLA shows a possible gas metallicity gradient of $\Delta Z/\Delta R = -0.02$ dex kpc^{-1} out to $R \approx 14$ kpc.

The bottom row of Fig. 4 presents a DLA at $d = 38$ kpc from an edge-on disk at $z = 0.525$. A strong velocity shear is also seen along the disk of this L_* galaxy. Because the QSO sightline occurs along the extended edge-on disk, Eq. (3) and (4) directly lead to $R \approx d$ and $v \approx v_{\rm obs}$ for this system. This DLA galaxy presents a second example for galaxies with an extended rotating disk out to ≈ 40 kpc. At the same time, the deep r-band image (lower-left panel) from *HST* suggests that the disk is warped near the QSO sightline, which is also reflected by the presence of a disturbed rotation velocity at $R > 5$ kpc (bottom-centre panel). The metallicity measured in the gas phase (bottom-right panel) displays a similar gradient of $\Delta Z/\Delta R = -0.02$ dex kpc^{-1} to the galaxy at the top, which is also comparable to what is seen in the ISM of nearby disk galaxies (e.g., Zaritsky et al 1994; van Zee et al 1998; Sánchez et al 2014). A declining gas-phase metallicity from the inner ISM to neutral gas at larger distances appears to hold for most DLA galaxies at $z \lesssim 1$ and the declining trend continues into ionized halo gas traced by strong LLS of $N(\mathrm{H\,I}) = 10^{19-20}\,\mathrm{cm}^{-2}$ (e.g., Péroux et al 2016).

At $z > 2$, spatially resolved observations of ISM gas kinematics become significantly more challenging, because the effective radii of L_* galaxies are typically $r_{\rm e} = 1-3$ kpc (e.g., Law et al 2012), corresponding to $\lesssim 0.3''$, and smaller for fainter or lower-mass objects. Star-forming regions in these distant galaxies are barely re-

solved in ground-based, seeing-limited observations (e.g., Law et al 2007; Förster Schreiber et al 2009; Wright et al 2009). Beam smearing can result in significant bias in interpreting the observed velocity shear and distributions of heavy elements (e.g., Davies et al 2011; Wuyts et al 2016). However, accurate measurements can be obtained to differentiate ISM metallicities of DLA galaxies from metallicities of neutral gas beyond the star-forming regions. Using the small sample of known DLA galaxies at $z \gtrsim 2$, a metallicity gradient of $\Delta Z/\Delta R = -0.02$ dex kpc^{-1} is also found in these distant star-forming galaxies (Christensen et al 2014; Jorgenson and Wolfe 2014).

4 The Star Formation Relation in the Early Universe

While direct identifications of galaxies giving rise to $z > 2$ DLAs have proven extremely challenging, critical insights into the star formation relation in the early Universe can still be gained from comparing the incidence of DLAs with the spatial distribution of star formation rate (SFR) per unit area uncovered in deep imaging data (Lanzetta et al 2002; Wolfe and Chen 2006). Specifically, the SFR per unit area ($\Sigma_{\rm SFR}$) is correlated with the surface mass density of neutral gas ($\Sigma_{\rm gas}$), following a Schmidt-Kennicutt relation in nearby galaxies (e.g., Schmidt 1959; Kennicutt 1998). The global star formation relation, $\Sigma_{\rm SFR} = 2.5\times10^{-4}\,(\Sigma_{\rm gas}/1\,M_\odot\,{\rm pc}^{-2})^{1.4}\,M_\odot\,{\rm yr}^{-1}\,{\rm kpc}^{-2}$ (dashed line in Fig. 5), is established using a sample of local spiral galaxies and nuclear starbursts (solid grey points in Fig. 5) over a broad range of $\Sigma_{\rm gas}$, from $\Sigma_{\rm gas} \approx 10\,M_\odot\,{\rm pc}^{-2}$ to $\Sigma_{\rm gas} \approx 10^4\,M_\odot\,{\rm pc}^{-2}$.

Empirical constraints for a Schmidt-Kennicutt relation at high redshifts require observations of the neutral gas content in star-forming galaxies. Although observations of individual galaxies in H I emission remain out of reach, the sample of $z = 1-3$ galaxies with resolved CO maps is rapidly growing (e.g., Baker et al 2004; Genzel et al 2010; Tacconi et al 2013). The observed $\Sigma_{\rm SFR}$ versus $\Sigma_{\rm molecular}$ for the high-redshift CO detected sample is shown in open squares in Fig. 5, which occur at high surface densities of $\Sigma_{\rm molecular} \gtrsim 100\,M_\odot\,{\rm pc}^{-2}$. Considering only $\Sigma_{\rm molecular}$ is appropriate for these galaxies, because locally it has been shown that at this high surface density regime molecular gas dominates (e.g., Martin and Kennicutt 2001; Wong and Blitz 2002; Bigiel et al 2008). In contrast, DLAs probe neutral gas with $N({\rm H\,I})$ ranging from $N({\rm H\,I}) = 2\times10^{20}\,{\rm cm}^{-2}$ to $N({\rm H\,I}) \approx 5\times10^{22}\,{\rm cm}^{-2}$. The range in $N({\rm H\,I})$ corresponds to a range in surface mass density of atomic gas from $\Sigma_{\rm atomic} \approx 2\,M_\odot\,{\rm pc}^{-2}$ to $\Sigma_{\rm atomic} \gtrsim 200\,M_\odot\,{\rm pc}^{-2}$, which is comparable to the global average of total neutral gas surface mass density in local disk galaxies (e.g., Fig. 5). Therefore, DLAs offer an important laboratory for investigating the star formation relation in the distant Universe, and direct constraints can be obtained from searches of *in situ* star formation in DLAs.

In principle, the Schmidt-Kennicutt relation can be rewritten in terms of $N({\rm H\,I})$ for pure atomic gas following

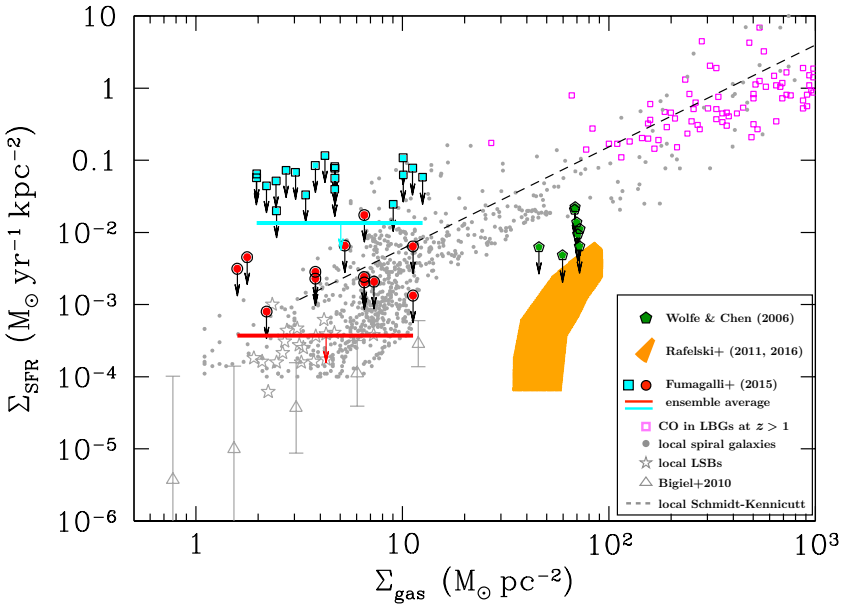

Fig. 5 The global star formation relation observed in nearby galaxies and at high redshifts. The correlation between the SFR per unit area ($\Sigma_{\rm SFR}$) and the total surface gas mass density ($\Sigma_{\rm gas}$), combining both atomic (H I) and molecular (H_2) for nearby spiral and starburst galaxies are shown in small filled circles (Kennicutt 1998; Graciá-Carpio et al 2008; Leroy et al 2008), together with the best-fit Schmidt-Kennicutt relation shown by the dashed line (Kennicutt 1998). A reduced star formation efficiency is observed both in low surface brightness galaxies and in the outskirts of normal spirals, which are shown in grey star symbols and open triangles, respectively (Wyder et al 2009; Bigiel et al 2010). CO molecules have been detected in many massive starburst galaxies ($M_{\rm star} > 2.5\times10^{10}\,M_\odot$) at $z = 1-3$ (e.g., Baker et al 2004; Genzel et al 2010; Tacconi et al 2013), which occur at the high surface density regime of the global star formation relation (open squares). In contrast, searching for *in situ* star formation in DLAs has revealed a reduced star formation efficiency in this metal-deficient gas. Specifically, green points and orange shaded area represent the constraints obtained from comparing the sky coverage of low surface brightness emission with the incidence of DLAs (Wolfe and Chen 2006; Rafelski et al 2011, 2016). Cyan squares and red circles represent the limits inferred from imaging searches of galaxies associated with individual DLAs, and the cyan and red bars represent the limiting $\Sigma_{\rm SFR}$ based on ensemble averages of the two samples (Fumagalli et al 2015). The level of star formation observed in high-N(H I) DLAs (green pentagons and orange shaded area) is comparable to what is seen in nearby low surface brightness galaxies and in the outskirts of normal spirals. See the main text for a detailed discussion

$$\Sigma_{\rm SFR} = K\times[N({\rm H\,I})/N_0]^\beta \quad M_\odot\,{\rm yr}^{-1}\,{\rm kpc}^{-2}, \tag{5}$$

which is justified for regions probed by DLAs with a low molecular gas content (see Sect. 2 and Fig. 3d). For reference, the local Schmidt-Kennicutt relation has $K = 2.5\times10^{-4}\,M_\odot\,{\rm yr}^{-1}\,{\rm kpc}^{-2}$, $\beta = 1.4$, and $N_0 = 1.25\times10^{20}\,{\rm cm}^{-2}$ for a pure atomic hydrogen gas. Following Eq. (5), the N(H I) distribution function, $f_{N({\rm H\,I})}$ (e.g., Fig. 3a), can then be expressed in terms of the $\Sigma_{\rm SFR}$ distribution function,

$h(\Sigma_{\rm SFR})$, which is the projected proper area per $d\Sigma_{\rm SFR}$ interval per comoving volume (Lanzetta et al 2002). The $\Sigma_{\rm SFR}$ distribution function $h(\Sigma_{\rm SFR})$ is related to $f_{N({\rm H\,I})}$ according to $h(\Sigma_{\rm SFR})\,d\Sigma_{\rm SFR} = (H_0/c)\,f_{N({\rm H\,I})}\,dN({\rm H\,I})$.

This exercise immediately leads to two important observable quantities. First, the sky covering fraction ($C_{\rm A}$) of star-forming regions in the redshift range, $[z_1, z_2]$, with an observed SFR per unit area in the interval of $\Sigma_{\rm SFR}$ and $\Sigma_{\rm SFR} + d\Sigma_{\rm SFR}$ is determined following

$$C_{\rm A}[\Sigma_{\rm SFR}|N({\rm H\,I})] = \int_{z_1}^{z_2} \frac{c\,(1+z)^2}{H(z)} h(\Sigma_{\rm SFR})\,d\Sigma_{\rm SFR}\,dz, \tag{6}$$

where c is the speed of light and $H(z)$ is the Hubble expansion rate. Equation (6) is equivalent to $f_{N({\rm H\,I})}dN({\rm H\,I})dX$, where $dX \equiv (1+z)^2 H_0/H(z)\,dz$ is the comoving absorption pathlength. In addition, the first moment of $h(\Sigma_{\rm SFR})$ leads to the comoving SFR density (Lanzetta et al 2002; Hopkins et al 2005),

$$\dot{\rho}_*(>\Sigma_{\rm SFR}^{\rm min}) = \int_{\Sigma_{\rm SFR}^{\rm min}}^{\Sigma_{\rm SFR}^{\rm max}} \Sigma_{\rm SFR} h(\Sigma_{\rm SFR})\,d\Sigma_{\rm SFR}. \tag{7}$$

Constraints on the star formation relation at high redshift, namely K and β in Eq. (5), can then be obtained by comparing $f_{N({\rm H\,I})}$-inferred $C_{\rm A}$ and $\dot{\rho}_*$ with results from searches of low surface brightness emission in deep galaxy survey data. Furthermore, estimates of missing light in low surface brightness regions can also be obtained using Eq. (7) (e.g., Lanzetta et al 2002; Rafelski et al 2011).

In practice, Eq. (5) is a correct representation only if disks are not well formed and a spherical symmetry applies to the DLAs. For randomly oriented disks, corrections for projection effects are necessary and detailed formalisms are presented in Wolfe and Chen (2006) and Rafelski et al (2011). In addition, the inferred surface brightness of *in situ* star formation in the DLA gas is extremely low after accounting for the cosmological surface brightness dimming. At $z = 2-3$, only DLAs at the highest-$N({\rm H\,I})$ end of $f_{N({\rm H\,I})}$ are expected to be visible in ultra-deep imaging data (cf. Lanzetta et al 2002; Wolfe and Chen 2006). For example, DLAs of $N({\rm H\,I}) > 1.6\times10^{21}\,{\rm cm}^{-2}$ at $z \approx 3$ are expected to have V-band (corresponding roughly to rest-frame 1500 Å at $z = 3$) surface brightness $\mu_V \lesssim 28.4$ mag arcsec^{-2}, assuming the local Schmidt-Kennicutt relation. The expected low surface brightness of UV photons from young stars in high-redshift DLAs dictates the galaxy survey depth necessary to uncover star formation associated with the DLA gas. At $N({\rm H\,I}) > 1.6\times10^{21}\,{\rm cm}^{-2}$, roughly 3% of the sky ($C_{\rm A} \approx 0.03$) is expected to be covered by extended low surface brightness emission of $\mu_V \lesssim 28.4$ mag arcsec^{-2}. For comparison, the sky covering fraction of luminous starburst galaxies at $z = 2-3$ is less than 0.1%.

Available constraints for the star formation efficiency at $z = 1-3$ are shown in colour symbols in Fig. 5. Specifically, the Hubble Ultra Deep Field (HUDF; Beckwith et al 2006) V-band image offers sufficient depth for detecting objects of $\mu_V \approx 28.4$ mag arcsec^{-2}. Under the assumption that DLAs originate in regions

distinct from known star-forming galaxies, an exhaustive search for extended low surface brightness emission in the HUDF has uncovered only a small number of these faint objects, far below the expectation from applying the local Schmidt-Kennicutt relation for DLAs of $N(\mathrm{H\,I}) > 1.6\times10^{21}\,\mathrm{cm}^{-2}$ following Eq. (6). Consequently, matching the observed limit on $\dot{\rho}_*$ from these faint objects with expectations from Eq. (7) has led to the conclusion that the star formation efficiency in metal-deficient atomic gas is more than $10\times$ lower than expectations from the local Schmidt-Kennicutt relation (Wolfe and Chen 2006; green pentagons in Fig. 5).

On the other hand, independent observations of DLA galaxies at $z = 2-3$ have suggested that these absorbers are associated with typical star-forming galaxies at high redshifts. These include a comparable clustering amplitude of DLAs and these galaxies (e.g., Cooke et al 2006), the findings of a few DLA galaxies with mass and SFR comparable to luminous star-forming galaxies found in deep surveys (e.g., Møller et al 2002, 2004; Christensen et al 2007), and detections of a DLA feature in the ISM of star-forming galaxies (e.g., Pettini et al 2002; Chen et al 2009; Dessauges-Zavadsky et al 2010). If DLAs originate in neutral gas around known star-forming galaxies, then these luminous star-forming galaxies should be more spatially extended than has been realized. Searches for low surface brightness emission in the outskirts of these galaxies based on stacked images have indeed uncovered extended low surface brightness emission out to more than twice the optical extent of a single image. However, repeating the exercise of computing the cumulative $\dot{\rho}_*$ from Eq. (7) has led to a similar conclusion that the star formation efficiency is more than $10\times$ lower in metal-deficient atomic gas at $z = 1-3$ than expectations from the local Schmidt-Kennicutt relation (Rafelski et al 2011, 2016). The results are shown as the orange shaded area in Fig. 5). In addition, the amount of missing light in the outskirts of these luminous star-forming galaxies is found to be $\approx 10\%$ of what is observed in the core (Rafelski et al 2011).

At the same time, imaging searches of individual DLA galaxies have been conducted for ≈ 30 DLAs identified along QSO sightlines that have high-redshift LLS serving as a natural coronograph to block the background QSO glare, improving the imaging depth in areas immediate to the QSO sightline (Fumagalli et al 2015). These searches have yielded only null results, leading to upper limits on the underlying surface brightness of the DLA galaxies (cyan squares and red circles in Fig. 5). While the survey depth is not sufficient for detecting associated star-forming regions in most DLAs in the survey sample of Fumagalli et al (2015) based on the local Schmidt-Kennicutt relation, the ensemble average is beginning to place interesting limits (cyan and red arrows).

The lack of *in situ* star formation in DLAs may not be surprising given the low molecular gas content. In the local Universe, it is understood that the Schmidt-Kennicutt relation is driven primarily by molecular gas mass ($\Sigma_{\mathrm{molecular}}$), while the surface density of atomic gas (Σ_{atomic}) "saturates" at $\sim 10 M_\odot\,\mathrm{pc}^{-2}$ beyond which the gas transitions into the molecular phase (e.g., Martin and Kennicutt 2001; Wong and Blitz 2002; Bigiel et al 2008). As described in Sect. 2 and Fig. 3d, the transitional surface density from atomic to molecular is metallicity dependent. Therefore, the low star formation efficiency observed in DLA gas can be understood as

a metallicity-dependent Schmidt-Kennicutt relation. This is qualitatively consistent with the observed low $\Sigma_{\rm SFR}$ in nearby low surface brightness galaxies (e.g., Wyder et al 2009; star symbols in Fig. 5) and in the outskirts of normal spirals (e.g., Bigiel et al 2010; open triangles in Fig. 5), where the ISM is found to be metal-poor (e.g., McGaugh 1994; Zaritsky et al 1994; Bresolin et al 2012). Numerical simulations incorporating a metallicity dependence in the H_2 production rate have also confirmed that the observed low star formation efficiency in DLAs can be reproduced in metal-poor gas (e.g., Gnedin and Kravtsov 2010).

A metallicity-dependent Schmidt-Kennicutt relation has wide-ranging implications in extragalactic research, from the physical origin of DLAs at high redshifts, to star formation and chemical enrichment histories in different environments, and to detailed properties of distant galaxies such as morphologies, sizes, and cold gas content. It is clear from Fig. 5 that there exists a significant gap in the gas surface densities, between $\Sigma_{\rm gas} \approx 10\,M_\odot\,{\rm pc}^{-2}$ probed by these direct DLA galaxy searches and $\Sigma_{\rm gas} \approx 100\,M_\odot\,{\rm pc}^{-2}$ probed by CO observations of high-redshift starburst systems (open squares in Fig. 5). Continuing efforts targeting high-N(H I) DLAs (and therefore high $\Sigma_{\rm gas}$) at sufficient imaging depths are expected to place critical constraints on the star formation relation in low-metallicity environments at high redshifts. Similarly, spatially resolved maps of star formation and neutral gas at $z > 1$ to mean surface densities of $\Sigma_{\rm SFR} < 0.1\,M_\odot\,{\rm yr}^{-1}\,{\rm kpc}^{-2}$ and $\Sigma_{\rm atomic,molecular} \approx 10-100\,M_\odot\,{\rm pc}^{-2}$ will bridge the gap of existing observations and offer invaluable insights into the star formation relation in different environments.

5 From Neutral ISM to the Ionized Circumgalactic Medium

Beyond the neutral ISM, strong Lyα absorbers of $N({\rm H\,I}) \approx 10^{14-20}\,{\rm cm}^{-2}$ and associated metal-line absorbers offer a sensitive probe of the diffuse circumgalactic medium (CGM) to projected distances $d \approx 100-500$ kpc (e.g., Fig. 2). But because the circumgalactic gas is significantly more ionized in the LLS and lower-N(H I) regime, measurements of its ionization state and metallicity bear considerable uncertainties and should be interpreted with caution.

Several studies have attempted to constrain the ionization state and metallicity of the CGM by considering the relative abundances of different ions at low- and high-ionization states (e.g., Savage et al 2002; Stocke et al 2006). For example, attributing observed O VI absorbers to cool ($T \sim 10^4$ K), photo-ionized gas irradiated by the metagalactic ionizing radiation field, the observed column density ratios between O VI and low-ionization transitions (such as C III and C IV) require extremely low gas densities of $n_{\rm H} \sim 10^{-5}\,{\rm cm}^{-3}$. Combining the inferred low gas density with observed N(O VI), which are typically $\gtrsim 10^{14.5}\,{\rm cm}^{-2}$ in galactic haloes (e.g., Tumlinson et al 2011), leads to a moderate gas metallicity of $\gtrsim 1/10$ Solar and unphysically large cloud sizes of $l_c \sim 1$ Mpc (e.g., Tripp et al 2001; Savage et al 2002; Stocke

et al 2006)[2]. Excluding O VI due to possible origins in shocks or turbulent mixing layers (e.g., Heckman et al 2002) and considering only relative abundances of low-ionization species increases estimated gas densities to $n_{\rm H} \sim 10^{-4} - 10^{-3}\,{\rm cm}^{-3}$. The inferred cloud sizes remain large with $l_c \sim 10 - 100\,{\rm kpc}$, in tension with what is observed locally for the HVCs. The implied thermal pressures in the cool gas phase are still two orders of magnitude lower than what is expected from pressure equilibrium with a hot ($T \approx 10^6$ K) medium (e.g., Stocke et al 2013; Werk et al 2014), indicating that these clouds would be crushed quickly. Considering non-equilibrium conditions (e.g., Gnat and Sternberg 2007; Oppenheimer and Schaye 2013) and the presence of local ionizing sources may help alleviate these problems (e.g., Cantalupo 2010), but the systematic uncertainties are difficult to quantify.

Nevertheless, exquisite details concerning extended halo gas have been learned over the past decade based on various samples of close galaxy and background QSO pairs. Because luminous QSOs are rare, roughly one QSO of $g \lesssim 18$ mag per square degree (e.g., Richards et al 2006), absorption-line studies of the CGM against background QSO light have been largely limited to one probe per galaxy. Only in a few cases are multiple QSOs found at $d \lesssim 300\,{\rm kpc}$ from a foreground galaxy (e.g., Norman et al 1996; Keeney et al 2013; Davis et al 2015; Lehner et al 2015; Bowen et al 2016) for measuring coherence in spatial distribution and kinematics of extended gas around the galaxy. All of these cases are in the local Universe, because the relatively large angular extent of these galaxies on the sky increases the probability of finding more than one background QSO. This local sample has now been complemented with new studies, utilizing multiply lensed QSOs and close projected QSO pairs, which provide spatially resolved CGM absorption properties for a growing sample of galaxies at intermediate redshifts (e.g., Chen et al 2014; Rubin et al 2015; Zahedy et al 2016).

With one QSO probe per halo, a two-dimensional map of CGM absorption properties can be established based on an ensemble average of a large sample of QSO-galaxy pairs ($N_{\rm pair} \sim 100 - 1000$). Fig.6 summarizes some of the observable quantities of the CGM. First, panels (a) and (b) at the top display the radial profiles of rest-frame absorption equivalent width ($W_{\rm r}$) for different absorption transitions, including hydrogen Lyα, low-ionization C II and Si II, intermediate-ionization Si III, Si IV, and C IV, and high-ionization O VI absorption transitions, colour-coded in black, red, orange, green, blue, magenta, and dark purple, respectively. For transitions that are not detected, a 2-σ upper limit is shown as a downward arrow. Because of the large number of data points, the upper limits are shown in pale colours for clarity. The galaxy sample includes 44 galaxies at $z \approx 0.25$ from the COS-Halos project (open squares; Tumlinson et al 2011, 2013; Werk et al 2013) and ~ 200 galaxies at $z \approx 0.04$ from public archives (circles; Liang and Chen 2014), for which high-quality, ultraviolet QSO spectra are available for constraining the presence or absence of multiple ions in individual haloes. These galaxies span four decades in total stellar mass, from $M_{\rm star} \approx 10^7 M_\odot$ to $M_{\rm star} \approx 10^{11} M_\odot$, and a wide range in

[2] For comparison, the sizes of extended HVC complexes at $d \sim 10\,{\rm kpc}$ from the MW disk are a few to 15 kpc across (e.g., Putman et al 2012). HVCs at larger distances are found to be more compact, $\lesssim 2\,{\rm kpc}$ (e.g., Westmeier et al 2008; Lockman et al 2012; Giovanelli et al 2013).

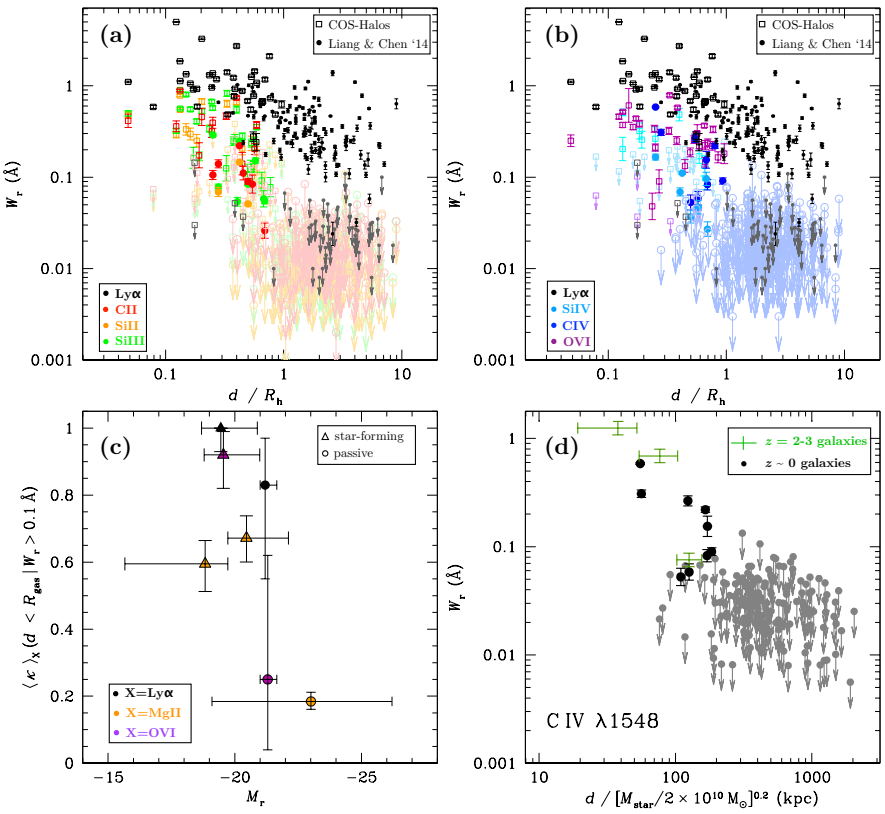

Fig. 6 Observed absorption properties of halo gas around galaxies. The *top* panels display the radial profiles of rest-frame absorption equivalent width (W_r) versus halo-radius R_h-normalized projected distance for different absorption transitions. Low-ionization transitions are presented in panel (*a*) and high-ionization transitions in panel (*b*). Lyα data points are presented in both panels for cross-comparison. The galaxy sample includes 44 galaxies at $z \approx 0.25$ from the COS-Halos project (open squares; Tumlinson et al 2011, 2013; Werk et al 2013) and ~ 200 galaxies at $z \approx 0.04$ from public archives (circles; Liang and Chen 2014), for which high-quality, ultraviolet QSO spectra are available for constraining the presence or absence of multiple ions in individual haloes. Different transitions are colour-coded to highlight the differences in their spatial distributions. For transitions that are not detected, a 2-σ upper limit is shown by a downward arrow. No heavy ions are found beyond $d = R_h$, while Lyα continues to be seen to larger distances. Panel (*c*) displays the ensemble average of gas covering fraction ($\langle \kappa \rangle$) as a function of absolute *r*-band magnitude (M_r) for Lyα (black symbols), Mg II (orange), and O VI (purple). Star-forming galaxies (triangles) on average are fainter and exhibit higher covering fractions of hydrogen and chemically enriched gas probed by both low- and high-ionization species than passive galaxies (circles). Measurements of Lyα- and O VI-absorbing gas are based on COS-Halos galaxies for $R_{gas} = R_h$. Measurements of Mg II-absorbing gas are based on ≈ 260 star-forming galaxies at $z \approx 0.25$ (Chen et al 2010a), and ~ 38000 passive luminious red galaxies at $z \approx 0.5$ (Huang et al 2016) for $R_{gas} = R_h/3$. Panel (*d*) illustrates the apparent constant nature of mass-normalized radial profiles of CGM absorption since $z \approx 3$ (e.g., Chen 2012; Liang and Chen 2014). The high-redshift observations are based on mean C IV absorption in stacked spectra of ~ 500 starburst galaxies with a mean stellar mass and dispersion of $\langle \log M_{star} \rangle = 9.9 \pm 0.5$ (Steidel et al 2010), and the low-redshift observations are for ~ 200 individual galaxies with $\langle \log M_{star} \rangle = 9.7 \pm 1.1$ and modest SFR (Liang and Chen 2014)

SFR, from SFR $< 0.1\,M_\odot\,\mathrm{yr}^{-1}$ to SFR $> 10\,M_\odot\,\mathrm{yr}^{-1}$. Diffuse gas is observed beyond $d = 50$ kpc around distant galaxies, extending the detection limit of H I gas in inner galactic haloes from 21 cm observations (e.g., Fig. 2) to lower column density gas at larger distances and higher redshifts.

While W_r is typically found to decline steadily with increasing d for all transitions (e.g., Chen 2012; Werk et al 2014), the scatters are large. Including the possibility that more massive haloes have more spatially extended halo gas, the halo radius R_h-normalized W_r-d distribution indeed displays substantially reduced scatters in the radial profiles shown in panels (a) and (b) of Fig. 6. A reduced scatter in the R_h-normalized W_r-d distribution indicates that galaxy mass plays a dominant role in driving the extent of halo gas. In addition, it also confirms that accurate associations between absorbers and absorbing galaxies have been found for the majority of the systems.

A particularly interesting feature in Fig. 6 is a complete absence of heavy ions beyond $d = R_\mathrm{h}$, while detections of Lyα continue to larger distances. The absence of heavy ions at $d > R_\mathrm{h}$, which is observed for a wide range of ionization states, strongly indicates that chemical enrichment is confined within individual galaxy haloes. This finding applies to both low-mass dwarfs and massive galaxies. However, it should also be noted that heavy ions are observed beyond R_h for galaxies with close neighbours (e.g., Borthakur et al 2013; Johnson et al 2015), suggesting that environmental effects play a role in distributing heavy elements beyond the enriched gaseous haloes of individual galaxies. Comparing panels (a) and (b) of Fig. 6 also shows that within individual galaxy haloes, a global ionization gradient is seen with more highly ionized gas detected at larger distances. For instance, the observed W_r declines to < 0.1 Å at $d \approx 0.5\,R_\mathrm{h}$ for C II and Si II, while C IV and O VI absorbers of $W_\mathrm{r} > 0.1$ Å continue to be found beyond $0.5\,R_\mathrm{h}$.

The observed W_r versus d (or d/R_h) based on a blind survey of absorption features in the vicinities of known galaxies also enables measurements of gas covering fraction[3]. The mean gas covering fraction ($\langle\kappa\rangle$) can be measured by a simple accounting of the fraction of galaxies in an annular area displaying associated absorbers with W_r exceeding some detection threshold W_0, and uncertainties can be estimated based on a binomial distribution function. Dividing the sample into different projected distance bins, it is clear from Fig. 6a and b that the fraction of non-detections increases with increasing projected distance, resulting in a declining $\langle\kappa\rangle$ with increasing d for all transitions observed (see also Chen et al 2010a; Werk et al 2014; Huang et al 2016).

It is also interesting to examine how $\langle\kappa\rangle$ depends on galaxy properties. Figure 6c displays $\langle\kappa\rangle$ observed within a fiducial gaseous radius R_gas for star-forming (tri-

[3] A blind survey of absorption features around known galaxies differs fundamentally from a blind survey of galaxies around known absorbers (e.g., Kacprzak et al 2008). By design, a blind galaxy survey around known absorbers excludes transparent sightlines and does not provide the sample necessary for measuring the incidence and covering fraction of absorbing species. In addition, because of limited survey depths, a blind galaxy survey is more likely to find more luminous members at larger d that are correlated with the true absorbing galaxies which are fainter and closer to the QSO sightline, resulting in a significantly larger scatter in the W_r versus d distribution (e.g., Kacprzak et al 2008; Nielsen et al 2013).

angles) and passive (circles) galaxies. The measurements are made for Lyα (black symbols), Mg II (orange), and O VI (purple) with a threshold of $W_0 = 0.1$ Å, and shown in relation to the absolute r-band magnitude (M_r). Error bars represent the 68% confidence interval. The absolute r-band magnitude is a direct observable of a galaxy and serves as a proxy for its underlying total stellar mass. Measurements of Lyα- and O VI-absorbing gas are based on COS-Halos galaxies for $R_{\rm gas} = R_{\rm h}$ (see also Johnson et al 2015 for a sample compiled from the literature). Measurements of Mg II-absorbing gas are based on ≈ 260 star-forming galaxies at $z \approx 0.25$ (Chen et al 2010a, and ~ 38000 passive luminous red galaxies at $z \approx 0.5$ (Huang et al 2016) for $R_{\rm gas} = R_{\rm h}/3$ (e.g., Chen and Tinker 2008). The larger sample sizes led to better constrained $\langle \kappa \rangle$ for Mg II absorbing gas in galactic haloes. In general, star-forming galaxies on average are fainter, less massive, and exhibit a higher covering fraction of chemically enriched gas than passive galaxies (see also Johnson et al 2015). At the same time, the covering fraction of chemically enriched gas is definitely non-zero around massive quiescent galaxies.

Comparing the radial profiles of CGM absorption at different redshifts offers additional insights into the evolution history of the CGM, which in turn helps distinguish between different models for chemical enrichment in galaxy haloes. The radial profiles of the CGM have been found to evolve little since $z \sim 3$ (e.g., Chen 2012), even though the star-forming properties in galaxies have evolved significantly. Figure 6d illustrates the apparent constant nature of mass-normalized radial profiles of C IV absorption in galactic haloes (Liang and Chen 2014). The high-redshift observations are based on stacked spectra of ~ 500 starburst galaxies with a mean stellar mass and dispersion of $\langle \log M_{\rm star} \rangle = 9.9 \pm 0.5$ (Steidel et al 2010) and a mean SFR of $\langle {\rm SFR} \rangle \approx 30 - 60 M_\odot\,{\rm yr}^{-1}$ (e.g., Erb et al 2006b; Reddy et al 2012). The low-redshift galaxy sample contains individual measurements of ~ 200 galaxies with $\langle \log M_{\rm star} \rangle = 9.7 \pm 1.1$ and more quiescent star-forming activities of $\langle {\rm SFR} \rangle \sim 1 M_\odot\,{\rm yr}^{-1}$ (Chen 2012; Liang and Chen 2014). The constant mass-normalized CGM radial profiles between galaxies of very different SFR indicate that mass (rather than SFR) is a dominant factor that determines the CGM properties over a cosmic time interval. This is consistent with previous findings that CGM absorption properties depend strongly on galaxy mass but only weakly on SFR (e.g., Chen et al 2010b), but at odds with popular models that attribute metal-line absorbers to starburst-driven outflows (e.g., Steidel et al 2010; Ménard et al 2011).

A discriminating characteristic of starburst-driven outflows is their distinctly non-spherical distribution in galactic haloes in the presence of a well-formed star-forming disk. Specifically, galactic-scale outflows are expected to travel preferentially along the polar axis where the gas experiences the least resistance (e.g., Heckman et al 1990). In contrast, accretion of the IGM is expected to proceed along the disk plane with $\lesssim 10\%$ covering fraction on the sky (e.g., Faucher-Giguère and Kereš 2011; Fumagalli et al 2011). Such azimuthal dependence of the spatial distribution of infalling and outflowing gas is fully realized in state-of-the-art cosmological zoom-in simulations (e.g., Shen et al 2013; Agertz and Kravtsov 2015). Observations of $z \approx 0.7$ galaxies have shown that at $d < 50$ kpc the mean Mg II ab-

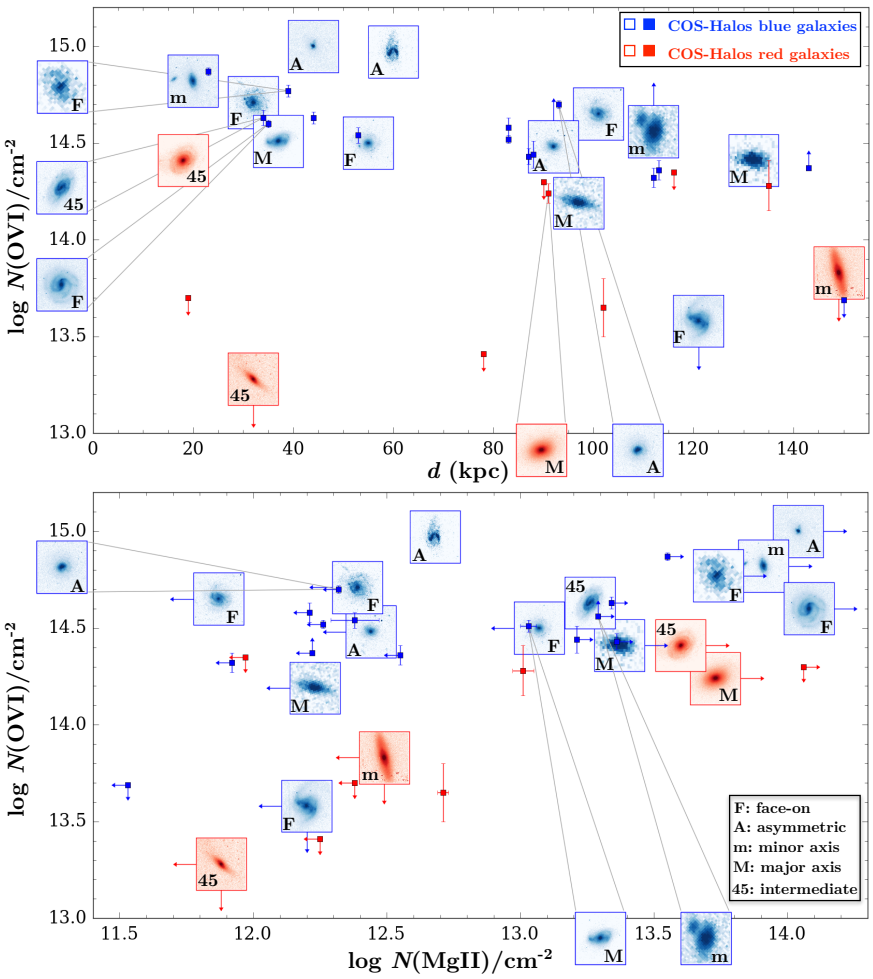

Fig. 7 Visual comparisons of the geometric alignment of galaxy major axis relative to the QSO sightline and the observed CGM absorption strength (by Rebecca Pierce). *Top*: Observed O VI column density, N(O VI), versus d for COS-Halos star-forming (in blue) and passive (in red) galaxies (Tumlinson et al 2011). *Bottom*: Comparisons of N(O VI) and N(Mg II) for the COS-Halos galaxies from Werk et al (2013). When spatially resolved images are available, the data points are replaced with an image panel of the absorbing galaxy. Each panel is 25 proper kpc on a side, and is oriented such that the QSO sightline occurs on the y-axis at the corresponding O VI column density of the galaxy. Disk alignments cannot be determined for face-on galaxies (minor-to-major axis ratio > 0.7) and galaxies displaying irregular/asymmetric morphologies, which are labeled "F" and "A", respectively. Galaxies with the QSO located within 30° of the minor axis are labeled 'm' in the lower-left corner, while galaxies with the QSO located within 30° of the major axis are labeled 'M'. Galaxies with the QSO sightline occuring intermediate ($30° - 60°$) between the minor and major axis are labeled "45". Downward arrows indicate 2-σ upper limits for non-detections, while upward arrows indicate saturated absorption lines. The COS-Halos galaxy sample provides a unique opportunity to examine low- and high-ionization halo gas for the same galaxies at once. Galaxies surrounded by O VI and Mg II absorbing gas clearly exhibit a broad range both in morphology and in disk orientation. In addition, the observed N(Mg II) displays a significantly larger scatter than N(O VI)

sorption equivalent width within 45° of the minor axis is twice of the mean value found within 45° of the major axis, although such azimuthal dependence is not observed at $d > 50$ kpc (Bordoloi et al 2011). The observed azimuthal dependence of the mean Mg II absorption strength is qualitatively consistent with the expectation that these heavy ions originate in starburst-driven outflows, and the lack of such azimuthal dependence implies that starburst outflows are confined to the inner halo of $d \lesssim 50$ kpc.

Many subsequent studies have generalized this observed azimuthal dependence at $d < 50$ kpc to larger distances and attributed absorbers detected near the minor axis to starburst-driven outflows and those found near the major axis to accretion (e.g., Bouché et al 2012; Kacprzak et al 2015). However, a causal connection between the observed absorbing gas and either outflows or accretion remains to be established. While gas metallicity may serve as a discriminator with the expectation of starburst outflows being more metal-enriched relative to the low-density IGM, uncertainties arise due to poorly understood chemical mixing and metal transport (e.g., Tumlinson 2006). Incidentally, a relatively strong Mg II absorber has been found at $d \approx 60$ kpc along the minor axis of a starburst galaxy but the metallicity of the absorbing gas is 10 times lower than what is observed in the ISM (Kacprzak et al 2014), highlighting the caveat of applying gas metallicity as the sole parameter for distinguishing between accretion and outflows.

Figure 7 presents visual comparisons of the geometric alignment of galaxy major axis relative to the QSO sightline and the observed CGM absorption strength. The figure at the top displays the observed O VI column density, $N(\mathrm{O\,VI})$, versus d for COS-Halos galaxies at $z \approx 0.2$ (Tumlinson et al 2013). The bottom figure displays comparisons of $N(\mathrm{O\,VI})$ and $N(\mathrm{Mg\,II})$ for these galaxies. The absorption-line measurements are adopted from Werk et al (2013). When spatially resolved images are available, the data points are replaced with an image panel of the absorbing galaxy. Each panel is 25 proper kpc on a side, and is oriented such that the QSO sightline falls on the y-axis at the corresponding $N(\mathrm{O\,VI})$ of the galaxy. The relative alignment between galaxy major axis and the background QSO sightline cannot be determined, if the galaxies are face-on with a minor-to-major axis ratio > 0.7 or if the galaxies display irregular/asymmetric morphologies. These galaxies are labeled "F" and "A", respectively. For galaxies that clearly display a smooth and elongated morphology, the orietation of the major axis can be accurately measured. Galaxies with the QSO located within 30° of the minor axis are labeled 'm', while galaxies with the QSO located within 30° of the major axis are labeled 'M'. Galaxies with the QSO sightline occuring intermediate ($30° - 60°$) between the minor and major axis are labeled "45". Star-forming galaxies are colour-coded in blue, and passive galaxies in red. Downward arrows indicate 2-σ upper limits for non-detections, while upward arrows indicate saturated absorption lines.

While the COS-Halos sample is small, particularly when restricting to those galaxies displaying a smooth, elongated morphology, it provides a unique opportunity to examine low- and high-ionization halo gas for the same galaxies at once. Two interesting features are immediately clear in Fig. 7. First, galaxies surrounded by O VI and Mg II absorbing gas exhibit a broad range both in morphology and in star

formation history, from compact quiescent galaxies, to regular star-forming disks, and to interacting pairs. The diverse morphologies in O VI and Mg II absorbing galaxies illuminate the challenge and uncertainties in characterizing their relative geometric orientation to the QSO sightline based on azimuthal angle alone. When considering only galaxies with smooth and elongated (minor-to-major axis ratio < 0.7) morphologies, no clear dependence of $N(\mathrm{O\,VI})$ or $N(\mathrm{Mg\,II})$ on galaxy orientation is found. Specifically, nine star-forming galaxies displaying strong O VI absorption at $d < 80$ kpc ($\log N(\mathrm{O\,VI})$) have spatially resolved images available. Two of these galaxies display disturbed morphologies and four are nearly face-on. The remaining three galaxies have the inclined disks oriented at 0°, 45°, and 90° each. For passive red galaxies, two have spatially resolved images available and both are elongated and aligned at $\approx 45^\circ$ from the QSO sightline. One displays an associated strong O VI absorber and the other has no corresponding O VI detections. At $d > 80$ kpc, the morphology distribution is similar to those at smaller distances. No strong dependence is found between the presence or absence of a strong O VI absorber and the galaxy orientation.

In addition, while the observed $N(\mathrm{O\,VI})$ at $d < 100\,kpc$ appears to be more uniformly distributed with a mean and scatter of $\log N(\mathrm{O\,VI}) = 14.5 \pm 0.3$ (Tumlinson et al 2011), the observed $N(\mathrm{Mg\,II})$ displays a significantly larger scatter. Specifically, the face-on galaxy at $d \approx 32$ kpc with an associated O VI absorber of $\log N(\mathrm{O\,VI}) \approx 14.7$ does not have an associated Mg II absorber detected to a limit of $\log N(\mathrm{Mg\,II}) \approx 12.4$. Two quiescent galaxies at $z \approx 20$ and 90 kpc (red panels) exhibit saturated Mg II absorption of $\log N(\mathrm{Mg\,II}) > 13.5$ and similarly strong O VI of $\log N(\mathrm{O\,VI}) \approx 14.3$. A small scatter implies a more uniformly distributed medium, while a large scatter implies a more clumpy nature of the absorbing gas or a larger variation between different galaxy haloes. Such distinct spatial distributions between low- and high-ionization gas further highlight the complex nature of the chemically enriched CGM, which depends on more than the geometric alignment of the galaxies. A three-dimensional model of gas kinematics that takes full advantage of the detailed morphologies and star formation history of the galaxies is expected to offer a deeper understanding of the physical origin of chemically enriched gas in galaxy haloes (e.g., Gauthier and Chen 2012; Chen et al 2014; Diamond-Stanic et al 2016).

6 Summary

QSO absorption spectroscopy provides a sensitive probe of both neutral medium and diffuse ionized gas in the distant Universe. It extends 21 cm maps of gaseous structures around low-redshift galaxies both to lower gas column densities and to higher redshifts. Specifically, DLAs of $N(\mathrm{H\,I}) \gtrsim 2 \times 10^{20}\,\mathrm{cm}^{-2}$ probe neutral gas in the ISM of distant star-forming galaxies, LLS of $N(\mathrm{H\,I}) > 10^{17}\,\mathrm{cm}^{-2}$ probe optically thick HVCs and gaseous streams in and around galaxies, and strong Lyα absorbers of $N(\mathrm{H\,I}) \approx 10^{14-17}\,\mathrm{cm}^{-2}$ and associated metal-line absorption transitions, such as

Mg II, C IV, and O VI, trace chemically enriched, ionized gas and starburst outflows. Over the last decade, an unprecedentedly large number of $\sim$ 10000 DLAs have been identified along random QSO sightlines to provide robust statistical characterizations of the incidence and mass density of neutral atomic gas at $z \lesssim 5$. Extensive follow-up studies have yielded accurate measurements of chemical compositions and molecular gas content for this neutral gas cross-section selected sample from $z \approx 5$ to $z \approx 0$ (Sect. 2). Combining galaxy surveys with absorption-line observations of gas around galaxies has enabled comprehensive studies of baryon cycles between star-forming regions and low-density gas over cosmic time. DLAs, while being rare as a result of a small cross-section of neutral medium in the Universe, have offered a unique window into gas dynamics and chemical enrichment in the outskirts of star-forming disks (Sect. 3), as well as star formation physics at high redshifts (Sect. 4). Observations of strong Lyα absorbers and associated ionic transitions around galaxies have also demonstrated that galaxy mass is a dominant factor in driving the extent of chemically enriched halo gas and that chemical enrichment is well confined within galactic haloes for both low-mass dwarfs and massive galaxies (Sect. 5).

With new observations carried out using new, multiplex instruments, continuing progress is expected in further advancing our understanding of baryonic cycles in the outskirts of galaxies over the next few years. These include, but are not limited to: (1) direct constraints for the star formation relation in different environments (e.g., Gnedin and Kravtsov 2010), particularly for star-forming galaxies at $z \gtrsim 2$ in low surface density regimes of $\Sigma_{\rm SFR} < 0.1\,M_\odot\,{\rm yr}^{-1}\,{\rm kpc}^{-2}$ and $\Sigma_{\rm gas} \approx 10-100\,M_\odot\,{\rm pc}^{-2}$; (2) an empirical understanding of galaxy environmental effects in distributing heavy elements to large distances based on deep galaxy surveys carried out in a large number of QSO fields (e.g., Johnson et al 2015); and (3) a three-dimensional map of gas flows in the circumgalactic space that combines absorption-line kinematics along multiple sightlines with optical morphologies of the absorbing galaxies and emission morphologies of extended gas around the galaxies (e.g., Rubin et al 2011; Chen et al 2014; Zahedy et al 2016). Wide-field IFUs on existing large ground-based telescopes substantially increase the efficiency in faint galaxy surveys (e.g., Bacon et al 2015) and in revealing extended low surface brightness emission features around high-redshift galaxies (e.g., Cantalupo et al 2014; Borisova et al 2016). The *James Webb Space Telescope* (*JWST*), which is scheduled to be launched in October 2018, will expand the sensitivity of detecting faint star-forming galaxies in the early Universe. Combining deep infrared images from *JWST* and CO (or dust continuum) maps from ALMA will lead to critical constraints for the star formation relation in low surface density regimes.

Acknowledgements The author wishes to dedicate this review to the memory of Arthur M. Wolfe for his pioneering and seminal work on the subject of damped Lyα absorbers and for inspiring generations of scientists to pursue original and fundamental research. The author thanks Nick Gnedin, Sean Johnson, Rebecca Pierce, Marc Rafelski, and Fakhri Zahedy for providing helpful input and comments. In preparing this review, the author has made use of NASA's Astrophysics Data System Bibliographic Services.

References

Agertz O, Kravtsov AV (2015) On the Interplay between Star Formation and Feedback in Galaxy Formation Simulations. ApJ804:18, DOI 10.1088/0004-637X/804/1/18, 1404.2613

Agertz O, Teyssier R, Moore B (2009) Disc formation and the origin of clumpy galaxies at high redshift. MNRAS397:L64–L68, DOI 10.1111/j.1745-3933.2009.00685.x, 0901.2536

Aguirre A, Dow-Hygelund C, Schaye J, Theuns T (2008) Metallicity of the Intergalactic Medium Using Pixel Statistics. IV. Oxygen. ApJ689:851-864, DOI 10.1086/592554, 0712.1239

Altay G, Theuns T, Schaye J, Crighton NHM, Dalla Vecchia C (2011) Through Thick and Thin–H I Absorption in Cosmological Simulations. ApJL737:L37, DOI 10.1088/2041-8205/737/2/L37, 1012.4014

Altay G, Theuns T, Schaye J, Booth CM, Dalla Vecchia C (2013) The impact of different physical processes on the statistics of Lyman-limit and damped Lyman α absorbers. MNRAS436:2689–2707, DOI 10.1093/mnras/stt1765, 1307.6879

Bacon R, Brinchmann J, Richard J, Contini T, Drake A, Franx M, Tacchella S, Vernet J, Wisotzki L, Blaizot J, Bouché N, Bouwens R, Cantalupo S, Carollo CM, Carton D, Caruana J, Clément B, Dreizler S, Epinat B, Guiderdoni B, Herenz C, Husser TO, Kamann S, Kerutt J, Kollatschny W, Krajnovic D, Lilly S, Martinsson T, Michel-Dansac L, Patricio V, Schaye J, Shirazi M, Soto K, Soucail G, Steinmetz M, Urrutia T, Weilbacher P, de Zeeuw T (2015) The MUSE 3D view of the Hubble Deep Field South. A&A575:A75, DOI 10.1051/0004-6361/201425419, 1411.7667

Baker AJ, Tacconi LJ, Genzel R, Lehnert MD, Lutz D (2004) Molecular Gas in the Lensed Lyman Break Galaxy cB58. ApJ604:125–140, DOI 10.1086/381798, astro-ph/0312099

Balestra I, Tozzi P, Ettori S, Rosati P, Borgani S, Mainieri V, Norman C, Viola M (2007) Tracing the evolution in the iron content of the intra-cluster medium. A&A462:429–442, DOI 10.1051/0004-6361:20065568, astro-ph/0609664

Beckwith SVW, Stiavelli M, Koekemoer AM, Caldwell JAR, Ferguson HC, Hook R, Lucas RA, Bergeron LE, Corbin M, Jogee S, Panagia N, Robberto M, Royle P, Somerville RS, Sosey M (2006) The Hubble Ultra Deep Field. AJ132:1729–1755, DOI 10.1086/507302, astro-ph/0607632

Bergeron J, Boissé P (1991) A sample of galaxies giving rise to Mg II quasar absorption systems. A&A243:344–366

Bergeron J, Stasińska G (1986) Absorption line systems in QSO spectra - Properties derived from observations and from photoionization models. A&A169:1–13

Bigiel F, Leroy A, Walter F, Brinks E, de Blok WJG, Madore B, Thornley MD (2008) The Star Formation Law in Nearby Galaxies on Sub-Kpc Scales. AJ136:2846–2871, DOI 10.1088/0004-6256/136/6/2846, 0810.2541

Bigiel F, Leroy A, Walter F, Blitz L, Brinks E, de Blok WJG, Madore B (2010) Extremely Inefficient Star Formation in the Outer Disks of Nearby Galaxies. AJ140:1194–1213, DOI 10.1088/0004-6256/140/5/1194, 1007.3498

Bird S, Vogelsberger M, Haehnelt M, Sijacki D, Genel S, Torrey P, Springel V, Hernquist L (2014) Damped Lyman α absorbers as a probe of stellar feedback. MNRAS445:2313–2324, DOI 10.1093/mnras/stu1923, 1405.3994

Boksenberg A, Sargent WLW (2015) Properties of QSO Metal-line Absorption Systems at High Redshifts: Nature and Evolution of the Absorbers and New Evidence on Escape of Ionizing Radiation from Galaxies. ApJS218:7, DOI 10.1088/0067-0049/218/1/7, 1410.3784

Bordoloi R, Lilly SJ, Knobel C, Bolzonella M, Kampczyk P, Carollo CM, Iovino A, Zucca E, Contini T, Kneib JP, Le Fevre O, Mainieri V, Renzini A, Scodeggio M, Zamorani G, Balestra I, Bardelli S, Bongiorno A, Caputi K, Cucciati O, de la Torre S, de Ravel L, Garilli B, Kovač K, Lamareille F, Le Borgne JF, Le Brun V, Maier C, Mignoli M, Pello R, Peng Y, Perez Montero E, Presotto V, Scarlata C, Silverman J, Tanaka M, Tasca L, Tresse L, Vergani D, Barnes L, Cappi A, Cimatti A, Coppa G, Diener C, Franzetti P, Koekemoer A, López-Sanjuan C, McCracken HJ, Moresco M, Nair P, Oesch P, Pozzetti L, Welikala N (2011) The Radial and Azimuthal Profiles of Mg II Absorption around $0.5 < z < 0.9$ zCOSMOS Galaxies of Different Colors, Masses, and Environments. ApJ743:10, DOI 10.1088/0004-637X/743/1/10, 1106.0616

Borisova E, Cantalupo S, Lilly SJ, Marino RA, Gallego SG, Bacon R, Blaizot J, Bouché N, Brinchmann J, Carollo CM, Caruana J, Finley H, Herenz EC, Richard J, Schaye J, Straka LA, Turner ML, Urrutia T, Verhamme A, Wisotzki L (2016) Ubiquitous giant Ly α nebulae around the brightest quasars at $z \sim 3.5$ revealed with MUSE. ArXiv e-prints 1605.01422

Borthakur S, Heckman T, Strickland D, Wild V, Schiminovich D (2013) The Impact of Starbursts on the Circumgalactic Medium. ApJ768:18, DOI 10.1088/0004-637X/768/1/18, 1303.1183

Bouché N, Hohensee W, Vargas R, Kacprzak GG, Martin CL, Cooke J, Churchill CW (2012) Physical properties of galactic winds using background quasars. MNRAS426:801–815, DOI 10.1111/j.1365-2966.2012.21114.x, 1110.5877

Bowen DV, Chelouche D, Jenkins EB, Tripp TM, Pettini M, York DG, Frye BL (2016) The Structure of the Circumgalactic Medium of Galaxies: Cool Accretion Inflow Around NGC 1097. ApJ826:50, DOI 10.3847/0004-637X/826/1/50, 1605.04907

Braun R (2012) Cosmological Evolution of Atomic Gas and Implications for 21 cm H I Absorption. ApJ749:87, DOI 10.1088/0004-637X/749/1/87, 1202.1840

Bresolin F, Kennicutt RC, Ryan-Weber E (2012) Gas Metallicities in the Extended Disks of NGC 1512 and NGC 3621. Chemical Signatures of Metal Mixing or Enriched Gas Accretion? ApJ750:122, DOI 10.1088/0004-637X/750/2/122, 1203.0956

Broeils AH, Rhee MH (1997) Short 21-cm WSRT observations of spiral and irregular galaxies. HI properties. A&A324:877–887

Burbidge EM, Burbidge GR (1961) Recent investigations of groups and clusters of galaxies. AJ66:541–550, DOI 10.1086/108461

Cantalupo S (2010) Stars quenching stars: how photoionization by local sources regulates gas cooling and galaxy formation. MNRAS403:L16–L20, DOI 10.1111/j.1745-3933.2010.00806.x, 0912.4149

Cantalupo S, Arrigoni-Battaia F, Prochaska JX, Hennawi JF, Madau P (2014) A cosmic web filament revealed in Lyman-α emission around a luminous high-redshift quasar. Nature506:63–66, DOI 10.1038/nature12898, 1401.4469

Cazaux S, Spaans M (2004) Molecular Hydrogen Formation on Dust Grains in the High-Redshift Universe. ApJ611:40–51, DOI 10.1086/422087, astro-ph/0404340

Chen HW (2012) The unchanging circumgalactic medium over the past 11 billion years. MNRAS427:1238–1244, DOI 10.1111/j.1365-2966.2012.22053.x, 1209.1094

Chen HW, Lanzetta KM (2003) The Nature of Damped Lyα Absorbing Galaxies at z <= 1: A Photometric Redshift Survey of Damped Lyα Absorbers. ApJ597:706–729, DOI 10.1086/378635, astro-ph/0308190

Chen HW, Prochaska JX (2000) The Origin of a Chemically Enriched Lyα Absorption System at Z = 0.167. ApJL543:L9–L13, DOI 10.1086/318179, astro-ph/0009001

Chen HW, Tinker JL (2008) The Baryon Content of Dark Matter Halos: Empirical Constraints from Mg II Absorbers. ApJ687:745-756, DOI 10.1086/591927, 0801.2169

Chen HW, Kennicutt RC Jr, Rauch M (2005) Abundance Profiles and Kinematics of Damped Lyα Absorbing Galaxies at z $<$ 0.651,. ApJ620:703–722, DOI 10.1086/427088, astro-ph/0411006

Chen HW, Perley DA, Pollack LK, Prochaska JX, Bloom JS, Dessauges-Zavadsky M, Pettini M, Lopez S, Dall'aglio A, Becker GD (2009) High-Redshift Starbursting Dwarf Galaxies Revealed by γ-Ray Burst Afterglows. ApJ691:152–174, DOI 10.1088/0004-637X/691/1/152, 0809.2608

Chen HW, Helsby JE, Gauthier JR, Shectman SA, Thompson IB, Tinker JL (2010a) An Empirical Characterization of Extended Cool Gas Around Galaxies Using Mg II Absorption Features. ApJ714:1521–1541, DOI 10.1088/0004-637X/714/2/1521, 1004.0705

Chen HW, Wild V, Tinker JL, Gauthier JR, Helsby JE, Shectman SA, Thompson IB (2010b) What Determines the Incidence and Extent of Mg II Absorbing Gas Around Galaxies? ApJL724:L176–L182, DOI 10.1088/2041-8205/724/2/L176, 1011.0735

Chen HW, Gauthier JR, Sharon K, Johnson SD, Nair P, Liang CJ (2014) Spatially resolved velocity maps of halo gas around two intermediate-redshift galaxies. MNRAS438:1435–1450, DOI 10.1093/mnras/stt2288, 1312.0016

Christensen L, Wisotzki L, Roth MM, Sánchez SF, Kelz A, Jahnke K (2007) An integral field spectroscopic survey for high redshift damped Lyman-α galaxies. A&A468:587–601, DOI 10.1051/0004-6361:20066410, 0704.0654

Christensen L, Møller P, Fynbo JPU, Zafar T (2014) Verifying the mass-metallicity relation in damped Lyman α selected galaxies at $0.1 < z < 3.2$. MNRAS445:225–238, DOI 10.1093/mnras/stu1726, 1404.6529

Chynoweth KM, Langston GI, Yun MS, Lockman FJ, Rubin KHR, Scoles SA (2008) Neutral Hydrogen Clouds in the M81/M82 Group. AJ135:1983–1992, DOI 10.1088/0004-6256/135/6/1983, 0803.3631

Cooke J, Wolfe AM, Gawiser E, Prochaska JX (2006) Survey for Galaxies Associated with z ˜ 3 Damped Lyα Systems. II. Galaxy-Absorber Correlation Functions. ApJ652:994–1010, DOI 10.1086/507476, astro-ph/0607149

Crighton NHM, Murphy MT, Prochaska JX, Worseck G, Rafelski M, Becker GD, Ellison SL, Fumagalli M, Lopez S, Meiksin A, O'Meara JM (2015) The neutral hydrogen cosmological mass density at z = 5. MNRAS452:217–234, DOI 10.1093/mnras/stv1182, 1506.02037

Davies R, Förster Schreiber NM, Cresci G, Genzel R, Bouché N, Burkert A, Buschkamp P, Genel S, Hicks E, Kurk J, Lutz D, Newman S, Shapiro K, Sternberg A, Tacconi LJ, Wuyts S (2011) How Well Can We Measure the Intrinsic Velocity Dispersion of Distant Disk Galaxies? ApJ741:69, DOI 10.1088/0004-637X/741/2/69, 1108.0285

Davis JD, Keeney BA, Danforth CW, Stocke JT (2015) On the Size and Mass of Photoionized Clouds in Extended Spiral Galaxy Halos. ApJ810:92, DOI 10.1088/0004-637X/810/2/92, 1506.04095

Decarli R, Walter F, Aravena M, Carilli C, Bouwens R, da Cunha E, Daddi E, Ivison RJ, Popping G, Riechers D, Smail I, Swinbank M, Weiss A, Anguita T, Assef R, Bauer F, Bell EF, Bertoldi F, Chapman S, Colina L, Cortes PC, Cox P, Dickinson M, Elbaz D, Gónzalez-López J, Ibar E, Infante L, Hodge J, Karim A, Le Fevre O, Magnelli B, Neri R, Oesch P, Ota K, Rix HW, Sargent M, Sheth K, van der Wel A, van der Werf P, Wagg J (2016) ALMA spectroscopic survey in the Hubble Ultra Deep Field: CO luminosity functions and the evolution of the cosmic density of molecular gas. ArXiv e-prints 1607.06770

Dessauges-Zavadsky M, D'Odorico S, Schaerer D, Modigliani A, Tapken C, Vernet J (2010) Rest-frame ultraviolet spectrum of the gravitationally lensed galaxy "the 8 o'clock arc": stellar and interstellar medium properties. A&A510:A26, DOI 10.1051/0004-6361/200913337, 0912.4384

Diamond-Stanic AM, Coil AL, Moustakas J, Tremonti CA, Sell PH, Mendez AJ, Hickox RC, Rudnick GH (2016) Galaxies Probing Galaxies at High Resolution: Co-rotating Gas Associated with a Milky Way Analog at z=0.4. ApJ824:24, DOI 10.3847/0004-637X/824/1/24, 1507.01945

D'Odorico V, Cristiani S, Pomante E, Carswell RF, Viel M, Barai P, Becker GD, Calura F, Cupani G, Fontanot F, Haehnelt MG, Kim TS, Miralda-Escudé J, Rorai A, Tescari E, Vanzella E (2016) Metals in the $z\sim3$ intergalactic medium: results from an ultra-high signal-to-noise ratio UVES quasar spectrum. MNRASDOI 10.1093/mnras/stw2161, 1608.06116

Elmegreen BG (1989) A pressure and metallicity dependence for molecular cloud correlations and the calibration of mass. ApJ338:178–196, DOI 10.1086/167192

Elmegreen BG (1993) The H to H2 transition in galaxies - Totally molecular galaxies. ApJ411:170–177, DOI 10.1086/172816

Erb DK, Shapley AE, Pettini M, Steidel CC, Reddy NA, Adelberger KL (2006a) The Mass-Metallicity Relation at z>˜2. ApJ644:813–828, DOI 10.1086/503623, astro-ph/0602473

Erb DK, Steidel CC, Shapley AE, Pettini M, Reddy NA, Adelberger KL (2006b) Hα Observations of a Large Sample of Galaxies at z ˜ 2: Implications for Star Formation in High-Redshift Galaxies. ApJ647:128–139, DOI 10.1086/505341, astro-ph/0604388

Erkal D, Gnedin NY, Kravtsov AV (2012) On the Origin of the High Column Density Turnover in the H I Column Density Distribution. ApJ761:54, DOI 10.1088/0004-637X/761/1/54, 1201.3653

Faucher-Giguère CA, Kereš D (2011) The small covering factor of cold accretion streams. MNRAS412:L118–L122, DOI 10.1111/j.1745-3933.2011.01018.x, 1011.1693

Fernández X, van Gorkom JH, Hess KM, Pisano DJ, Kreckel K, Momjian E, Popping A, Oosterloo T, Chomiuk L, Verheijen MAW, Henning PA, Schiminovich D, Bershady MA, Wilcots EM, Scoville N (2013) A Pilot for a Very Large Array H I Deep Field. ApJL770:L29, DOI 10.1088/2041-8205/770/2/L29, 1303.2659

Förster Schreiber NM, Genzel R, Bouché N, Cresci G, Davies R, Buschkamp P, Shapiro K, Tacconi LJ, Hicks EKS, Genel S, Shapley AE, Erb DK, Steidel CC, Lutz D, Eisenhauer F, Gillessen S, Sternberg A, Renzini A, Cimatti A, Daddi E, Kurk J, Lilly S, Kong X, Lehnert MD, Nesvadba N, Verma A, McCracken H, Arimoto N, Mignoli M, Onodera M (2009) The SINS Survey: SINFONI Integral Field Spectroscopy of z ˜ 2 Star-forming Galaxies. ApJ706:1364–1428, DOI 10.1088/0004-637X/706/2/1364, 0903.1872

Friis M, De Cia A, Krühler T, Fynbo JPU, Ledoux C, Vreeswijk PM, Watson DJ, Malesani D, Gorosabel J, Starling RLC, Jakobsson P, Varela K, Wiersema K, Drachmann AP, Trotter A, Thöne CC, de Ugarte Postigo A, D'Elia V, Elliott J, Maturi M, Goldoni P, Greiner J, Haislip J, Kaper L, Knust F, LaCluyze A, Milvang-Jensen B, Reichart D, Schulze S, Sudilovsky V, Tanvir N, Vergani SD (2015) The warm, the excited, and the molecular gas: GRB 121024A shining through its star-forming galaxy. MNRAS451:167–183, DOI 10.1093/mnras/stv960, 1409.6315

Fumagalli M, Prochaska JX, Kasen D, Dekel A, Ceverino D, Primack JR (2011) Absorption-line systems in simulated galaxies fed by cold streams. MNRAS418:1796–1821, DOI 10.1111/j.1365-2966.2011.19599.x, 1103.2130

Fumagalli M, O'Meara JM, Prochaska JX, Rafelski M, Kanekar N (2015) Directly imaging damped Ly α galaxies at z $>$ 2 - III. The star formation rates of neutral gas reservoirs at $z\sim$2.7. MNRAS446:3178–3198, DOI 10.1093/mnras/stu2325, 1409.2880

Gallazzi A, Brinchmann J, Charlot S, White SDM (2008) A census of metals and baryons in stars in the local Universe. MNRAS383:1439–1458, DOI 10.1111/j.1365-2966.2007.12632.x, 0708.0533

Gauthier JR, Chen HW (2012) Empirical constraints of supergalactic winds at $z \gtrsim$ 0.5. MNRAS424:1952–1962, DOI 10.1111/j.1365-2966.2012.21327.x, 1205.4037

Genzel R, Tacconi LJ, Gracia-Carpio J, Sternberg A, Cooper MC, Shapiro K, Bolatto A, Bouché N, Bournaud F, Burkert A, Combes F, Comerford J, Cox P, Davis M, Schreiber NMF, Garcia-Burillo S, Lutz D, Naab T, Neri R, Omont A, Shapley A, Weiner B (2010) A study of the gas-star formation relation over cosmic time. MNRAS407:2091–2108, DOI 10.1111/j.1365-2966.2010.16969.x, 1003.5180

Giovanelli R, Haynes MP, Adams EAK, Cannon JM, Rhode KL, Salzer JJ, Skillman ED, Bernstein-Cooper EZ, McQuinn KBW (2013) ALFALFA Discovery of the Nearby Gas-rich Dwarf Galaxy Leo P. I. H I Observations. AJ146:15, DOI 10.1088/0004-6256/146/1/15, 1305.0272

Gnat O, Sternberg A (2007) Time-dependent Ionization in Radiatively Cooling Gas. ApJS168:213–230, DOI 10.1086/509786, astro-ph/0608181

Gnedin NY, Draine BT (2014) Line Overlap and Self-Shielding of Molecular Hydrogen in Galaxies. ApJ795:37, DOI 10.1088/0004-637X/795/1/37, 1406.4129

Gnedin NY, Kravtsov AV (2010) On the Kennicutt-Schmidt Relation of Low-Metallicity High-Redshift Galaxies. ApJ714:287–295, DOI 10.1088/0004-637X/714/1/287, 0912.3005

Gnedin NY, Tassis K, Kravtsov AV (2009) Modeling Molecular Hydrogen and Star Formation in Cosmological Simulations. ApJ697:55–67, DOI 10.1088/0004-637X/697/1/55, 0810.4148

Graciá-Carpio J, García-Burillo S, Planesas P, Fuente A, Usero A (2008) Evidence of enhanced star formation efficiency in luminous and ultraluminous infrared galaxies. A&A479:703–717, DOI 10.1051/0004-6361:20078223, 0712.0582

Heckman TM, Armus L, Miley GK (1990) On the nature and implications of starburst-driven galactic superwinds. ApJS74:833–868, DOI 10.1086/191522

Heckman TM, Norman CA, Strickland DK, Sembach KR (2002) On the Physical Origin of O VI Absorption-Line Systems. ApJ577:691–700, DOI 10.1086/342232, astro-ph/0205556

Hopkins AM, Rao SM, Turnshek DA (2005) The Star Formation History of Damped Lyα Absorbers. ApJ630:108–114, DOI 10.1086/432046, astro-ph/0505418

Huang YH, Chen HW, Johnson SD, Weiner BJ (2016) Characterizing the chemically enriched circumgalactic medium of $\sim$ 38000 luminous red galaxies in SDSS DR12. MNRAS455:1713–1727, DOI 10.1093/mnras/stv2327, 1510.01336

Johnson SD, Chen HW, Mulchaey JS (2015) On the possible environmental effect in distributing heavy elements beyond individual gaseous haloes. MNRAS449:3263–3273, DOI 10.1093/mnras/stv553, 1503.04199

Jorgenson RA, Wolfe AM (2014) Spatially Resolved Emission of a High-redshift DLA Galaxy with the Keck/OSIRIS IFU. ApJ785:16, DOI 10.1088/0004-637X/785/1/16, 1311.0045

Jorgenson RA, Murphy MT, Thompson R, Carswell RF (2014) The Magellan uniform survey of damped Lyman α systems - II. Paucity of strong molecular hydrogen absorption. MNRAS443:2783–2800, DOI 10.1093/mnras/stu1314, 1407.1111

Kacprzak GG, Churchill CW, Steidel CC, Murphy MT (2008) Halo Gas Cross Sections and Covering Fractions of Mg II Absorption Selected Galaxies. AJ135:922-927, DOI 10.1088/0004-6256/135/3/922, 0710.5765

Kacprzak GG, Murphy MT, Churchill CW (2010) Galaxy group at z = 0.3 associated with the damped Lyman α system towards quasar Q1127-145. MNRAS406:445–459, DOI 10.1111/j.1365-2966.2010.16667.x, 1003.3669

Kacprzak GG, Martin CL, Bouché N, Churchill CW, Cooke J, LeReun A, Schroetter I, Ho SH, Klimek E (2014) New Perspective on Galaxy Outflows from the First Detection of Both Intrinsic and Traverse Metal-line Absorption. ApJL792:L12, DOI 10.1088/2041-8205/792/1/L12, 1407.4126

Kacprzak GG, Muzahid S, Churchill CW, Nielsen NM, Charlton JC (2015) The Azimuthal Dependence of Outflows and Accretion Detected Using O VI Absorption. ApJ815:22, DOI 10.1088/0004-637X/815/1/22, 1511.03275

Karachentsev ID, Kashibadze OG (2006) Masses of the local group and of the M81 group estimated from distortions in the local velocity field. Astrophysics 49:3–18, DOI 10.1007/s10511-006-0002-6

Keeney BA, Stocke JT, Rosenberg JL, Danforth CW, Ryan-Weber EV, Shull JM, Savage BD, Green JC (2013) HST/COS Spectra of Three QSOs That Probe the Circumgalactic Medium of a Single Spiral Galaxy: Evidence for Gas Recycling and Outflow. ApJ765:27, DOI 10.1088/0004-637X/765/1/27, 1301.4242

Kennicutt RC Jr (1998) The Global Schmidt Law in Star-forming Galaxies. ApJ498:541–552, DOI 10.1086/305588, astro-ph/9712213

Kereš D, Katz N, Fardal M, Davé R, Weinberg DH (2009) Galaxies in a simulated ΛCDM Universe - I. Cold mode and hot cores. MNRAS395:160–179, DOI 10.1111/j.1365-2966.2009.14541.x, 0809.1430

Kim TS, Partl AM, Carswell RF, Müller V (2013) The evolution of H I and C IV quasar absorption line systems at $1.9 < z < 3.2$. A&A552:A77, DOI 10.1051/0004-6361/201220042, 1302.6622

Krogager JK, Fynbo JPU, Møller P, Ledoux C, Noterdaeme P, Christensen L, Milvang-Jensen B, Sparre M (2012) On the sizes of $z \gtrsim 2$ damped Lyα absorbing galaxies. MNRAS424:L1–L5, DOI 10.1111/j.1745-3933.2012.01272.x, 1204.2833

Krühler T, Ledoux C, Fynbo JPU, Vreeswijk PM, Schmidl S, Malesani D, Christensen L, De Cia A, Hjorth J, Jakobsson P, Kann DA, Kaper L, Vergani SD, Afonso PMJ, Covino S, de Ugarte Postigo A, D'Elia V, Filgas R, Goldoni P, Greiner J, Hartoog OE, Milvang-Jensen B, Nardini M, Piranomonte S, Rossi A, Sánchez-Ramírez R, Schady P, Schulze S, Sudilovsky V, Tanvir NR, Tagliaferri G, Watson DJ, Wiersema K, Wijers RAMJ, Xu D (2013) Molecular hydrogen in the damped Lyman α system towards GRB 120815A at z = 2.36. A&A557:A18, DOI 10.1051/0004-6361/201321772, 1304.7003

Krumholz MR, McKee CF, Tumlinson J (2009) The Atomic-to-Molecular Transition in Galaxies. II: H I and H_2 Column Densities. ApJ693:216–235, DOI 10.1088/0004-637X/693/1/216, 0811.0004

Lanzetta KM, Wolfe AM, Turnshek DA, Lu L, McMahon RG, Hazard C (1991) A new spectroscopic survey for damped Ly-alpha absorption lines from high-redshift galaxies. ApJS77:1–57, DOI 10.1086/191596

Lanzetta KM, Yahata N, Pascarelle S, Chen HW, Fernández-Soto A (2002) The Star Formation Rate Intensity Distribution Function: Implications for the Cosmic Star Formation Rate History of the Universe. ApJ570:492–501, DOI 10.1086/339774, astro-ph/0111129

Law DR, Steidel CC, Erb DK, Larkin JE, Pettini M, Shapley AE, Wright SA (2007) Integral Field Spectroscopy of High-Redshift Star-forming Galaxies with Laser-guided Adaptive Optics: Evidence for Dispersion-dominated Kinematics. ApJ669:929–946, DOI 10.1086/521786, 0707.3634

Law DR, Steidel CC, Shapley AE, Nagy SR, Reddy NA, Erb DK (2012) An HST/WFC3-IR Morphological Survey of Galaxies at z = 1.5-3.6. I. Survey Description and Morphological Properties of Star-forming Galaxies. ApJ745:85, DOI 10.1088/0004-637X/745/1/85, 1107.3137

Ledoux C, Vreeswijk PM, Smette A, Fox AJ, Petitjean P, Ellison SL, Fynbo JPU, Savaglio S (2009) Physical conditions in high-redshift GRB-DLA absorbers observed with VLT/UVES: implications for molecular hydrogen searches. A&A506:661–675, DOI 10.1051/0004-6361/200811572, 0907.1057

Lehner N, Howk JC, Wakker BP (2015) Evidence for a Massive, Extended Circumgalactic Medium Around the Andromeda Galaxy. ApJ804:79, DOI 10.1088/0004-637X/804/2/79, 1404.6540

Lehnert MD, Heckman TM, Weaver KA (1999) Very Extended X-Ray and Hα Emission in M82: Implications for the Superwind Phenomenon. ApJ523:575–584, DOI 10.1086/307762, astro-ph/9904227

Leroy AK, Walter F, Brinks E, Bigiel F, de Blok WJG, Madore B, Thornley MD (2008) The Star Formation Efficiency in Nearby Galaxies: Measuring Where Gas Forms Stars Effectively. AJ136:2782–2845, DOI 10.1088/0004-6256/136/6/2782, 0810.2556

Leroy AK, Bolatto A, Gordon K, Sandstrom K, Gratier P, Rosolowsky E, Engelbracht CW, Mizuno N, Corbelli E, Fukui Y, Kawamura A (2011) The CO-to-H_2 Conversion Factor from Infrared Dust Emission across the Local Group. ApJ737:12, DOI 10.1088/0004-637X/737/1/12, 1102.4618

Liang CJ, Chen HW (2014) Mining circumgalactic baryons in the low-redshift universe. MNRAS445:2061–2081, DOI 10.1093/mnras/stu1901, 1402.3602

Lockman FJ, Free NL, Shields JC (2012) The Neutral Hydrogen Bridge between M31 and M33. AJ144:52, DOI 10.1088/0004-6256/144/2/52, 1205.5235

Lopez S, D'Odorico V, Ellison SL, Becker GD, Christensen L, Cupani G, Denney KD, Paris I, Worseck G, Berg TAM, Cristiani S, Dessauges-Zavadsky M, Haehnelt M, Hamann F, Hennawi J, Irsic V, Kim TS, Lopez P, Saust RL, Menard B, Perrotta S, Prochaska JX, Sanchez-Ramirez R, Vestergaard M, Viel M, Wisotzki L (2016) XQ-100: A legacy survey of one hundred $3.5 < z < 4.5$ quasars observed with VLT/XSHOOTER. ArXiv e-prints 1607.08776

Lu L, Sargent WLW, Barlow TA, Churchill CW, Vogt SS (1996) Abundances at High Redshifts: The Chemical Enrichment History of Damped Ly alpha Galaxies. ApJS107:475, DOI 10.1086/192373, astro-ph/9606044

Madau P, Dickinson M (2014) Cosmic Star-Formation History. ARA&A52:415–486, DOI 10.1146/annurev-astro-081811-125615, 1403.0007

Maiolino R, Nagao T, Grazian A, Cocchia F, Marconi A, Mannucci F, Cimatti A, Pipino A, Ballero S, Calura F, Chiappini C, Fontana A, Granato GL, Matteucci F, Pastorini G, Pentericci L, Risaliti G, Salvati M, Silva L (2008) AMAZE. I. The evolution of the mass-metallicity relation at z $>$ 3. A&A488:463–479, DOI 10.1051/0004-6361:200809678, 0806.2410

Mannucci F, Cresci G, Maiolino R, Marconi A, Pastorini G, Pozzetti L, Gnerucci A, Risaliti G, Schneider R, Lehnert M, Salvati M (2009) LSD: Lyman-break galaxies Stellar populations and Dynamics - I. Mass, metallicity and gas at z ˜ 3.1. MNRAS398:1915–1931, DOI 10.1111/j.1365-2966.2009.15185.x, 0902.2398

Marasco A, Crain RA, Schaye J, Bahé YM, van der Hulst T, Theuns T, Bower RG (2016) The environmental dependence of H I in galaxies in the EAGLE simulations. MNRAS461:2630–2649, DOI 10.1093/mnras/stw1498, 1606.06288

Martin CL, Kennicutt RC Jr (2001) Star Formation Thresholds in Galactic Disks. ApJ555:301–321, DOI 10.1086/321452, astro-ph/0103181

McGaugh SS (1994) Oxygen abundances in low surface brightness disk galaxies. ApJ426:135–149, DOI 10.1086/174049, astro-ph/9311064

Ménard B, Wild V, Nestor D, Quider A, Zibetti S, Rao S, Turnshek D (2011) Probing star formation across cosmic time with absorption-line systems. MNRAS417:801–811, DOI 10.1111/j.1365-2966.2011.18227.x, 0912.3263

Meyer DM, Welty DE, York DG (1989) Element abundances at high redshift. ApJL343:L37–L40, DOI 10.1086/185505

Møller P, Warren SJ, Fall SM, Fynbo JU, Jakobsen P (2002) Are High-Redshift Damped Lyα Galaxies Lyman Break Galaxies? ApJ574:51–58, DOI 10.1086/340934, astro-ph/0203361

Møller P, Fynbo JPU, Fall SM (2004) Detection of Lyman-α emission from a DLA galaxy: Possible implications for a luminosity-metallicity relation at z = 2-3. A&A422:L33–L37, DOI 10.1051/0004-6361:20040194, astro-ph/0406307

Muzahid S, Srianand R, Charlton J (2015) An HST/COS survey of molecular hydrogen in DLAs & sub-DLAs at z $<$ 1: molecular fraction and excitation temperature. MNRAS448:2840–2853, DOI 10.1093/mnras/stv133, 1410.3828

Neeleman M, Wolfe AM, Prochaska JX, Rafelski M (2013) The Fundamental Plane of Damped Lyα Systems. ApJ769:54, DOI 10.1088/0004-637X/769/1/54, 1303.7239

Neeleman M, Prochaska JX, Ribaudo J, Lehner N, Howk JC, Rafelski M, Kanekar N (2016a) The H I Content of the Universe Over the Past 10 GYRS. ApJ818:113, DOI 10.3847/0004-637X/818/2/113, 1601.01691

Neeleman M, Prochaska JX, Zwaan MA, Kanekar N, Christensen L, Dessauges-Zavadsky M, Fynbo JPU, van Kampen E, Møller P, Zafar T (2016b) First Connec-

tion between Cold Gas in Emission and Absorption: CO Emission from a Galaxy-Quasar Pair. ApJL820:L39, DOI 10.3847/2041-8205/820/2/L39, 1604.05720

Nielsen NM, Churchill CW, Kacprzak GG (2013) MAGIICAT II. General Characteristics of the Mg II Absorbing Circumgalactic Medium. ApJ776:115, DOI 10.1088/0004-637X/776/2/115, 1211.1380

Norman CA, Bowen DV, Heckman T, Blades C, Danly L (1996) Hubble Space Telescope Observations of QSO Absorption Lines Associated with Starburst Galaxy Outflows. ApJ472:73, DOI 10.1086/178042

Noterdaeme P, Ledoux C, Petitjean P, Srianand R (2008) Molecular hydrogen in high-redshift damped Lyman-α systems: the VLT/UVES database. A&A481:327–336, DOI 10.1051/0004-6361:20078780, 0801.3682

Noterdaeme P, Petitjean P, Ledoux C, Srianand R (2009) Evolution of the cosmological mass density of neutral gas from Sloan Digital Sky Survey II - Data Release 7. A&A505:1087–1098, DOI 10.1051/0004-6361/200912768, 0908.1574

Noterdaeme P, Petitjean P, Carithers WC, Pâris I, Font-Ribera A, Bailey S, Aubourg E, Bizyaev D, Ebelke G, Finley H, Ge J, Malanushenko E, Malanushenko V, Miralda-Escudé J, Myers AD, Oravetz D, Pan K, Pieri MM, Ross NP, Schneider DP, Simmons A, York DG (2012) Column density distribution and cosmological mass density of neutral gas: Sloan Digital Sky Survey-III Data Release 9. A&A547:L1, DOI 10.1051/0004-6361/201220259, 1210.1213

Noterdaeme P, Petitjean P, Srianand R (2015) The elusive HI$\rightarrow$H$_2$ transition in high-z damped Lyman-α systems. A&A578:L5, DOI 10.1051/0004-6361/201526018, 1505.04997

Noterdaeme P, Krogager JK, Balashev S, Ge J, Gupta N, Krühler T, Ledoux C, Murphy MT, Pâris I, Petitjean P, Rahmani H, Srianand R, Ubachs W (2016) Discovery of a Perseus-like cloud in the early Universe: HI-to-H2 transition, carbon monoxide and small dust grains at zabs=2.53 towards the quasar J0000+0048. ArXiv e-prints 1609.01422

Oosterloo T, Morganti R, Crocker A, Jütte E, Cappellari M, de Zeeuw T, Krajnović D, McDermid R, Kuntschner H, Sarzi M, Weijmans AM (2010) Early-type galaxies in different environments: an HI view. MNRAS409:500–514, DOI 10.1111/j.1365-2966.2010.17351.x, 1007.2059

Oppenheimer BD, Schaye J (2013) Non-equilibirum ionization and cooling of metal-enriched gas in the presence of a photoionization background. MNRAS434:1043–1062, DOI 10.1093/mnras/stt1043, 1302.5710

Péroux C, Bouché N, Kulkarni VP, York DG, Vladilo G (2011) A SINFONI integral field spectroscopy survey for galaxy counterparts to damped Lyman α systems - I. New detections and limits for intervening and associated absorbers. MNRAS410:2237–2250, DOI 10.1111/j.1365-2966.2010.17598.x, 1009.0025

Péroux C, Bouché N, Kulkarni VP, York DG, Vladilo G (2012) A SINFONI integral field spectroscopy survey for galaxy counterparts to damped Lyman α systems - III. Three additional detections. MNRAS419:3060–3073, DOI 10.1111/j.1365-2966.2011.19947.x, 1110.0666

Péroux C, Quiret S, Rahmani H, Kulkarni VP, Epinat B, Milliard B, Straka LA, York DG, Rahmati A, Contini T (2016) A SINFONI integral field spectroscopy

survey for galaxy counterparts to damped Lyman α systems - VI. Metallicity and geometry as gas flow probes. MNRAS457:903–916, DOI 10.1093/mnras/stw016, 1601.02796

Pettini M (2004) Element abundances through the cosmic ages. In: Esteban C, García López R, Herrero A, Sánchez F (eds) Cosmochemistry. The melting pot of the elements, pp 257–298, astro-ph/0303272

Pettini M, Boksenberg A, Hunstead RW (1990) Metal enrichment, dust, and star formation in galaxies at high redshifts. I - The Z = 2.3091 absorber toward PHL 957. ApJ348:48–56, DOI 10.1086/168212

Pettini M, Ellison SL, Steidel CC, Bowen DV (1999) Metal Abundances at z$<$1.5: Fresh Clues to the Chemical Enrichment History of Damped Lyα Systems. ApJ510:576–589, DOI 10.1086/306635, astro-ph/9808017

Pettini M, Shapley AE, Steidel CC, Cuby JG, Dickinson M, Moorwood AFM, Adelberger KL, Giavalisco M (2001) The Rest-Frame Optical Spectra of Lyman Break Galaxies: Star Formation, Extinction, Abundances, and Kinematics. ApJ554:981–1000, DOI 10.1086/321403, astro-ph/0102456

Pettini M, Rix SA, Steidel CC, Adelberger KL, Hunt MP, Shapley AE (2002) New Observations of the Interstellar Medium in the Lyman Break Galaxy MS 1512-cB58. ApJ569:742–757, DOI 10.1086/339355, astro-ph/0110637

Prochaska JX, Tumlinson J (2009) Baryons: What, When and Where? Astrophysics and Space Science Proceedings 10:419, DOI 10.1007/978-1-4020-9457-6_16, 0805.4635

Prochaska JX, Wolfe AM (1996) A Keck HIRES Investigation of the Metal Abundances and Kinematics of the Z = 2.46 Damped LY alpha System toward Q0201+365. ApJ470:403, DOI 10.1086/177875, astro-ph/9604042

Prochaska JX, Wolfe AM (1999) Chemical Abundances of the Damped Lyα Systems at z$>$1.5. ApJS121:369–415, DOI 10.1086/313200, astro-ph/9810381

Prochaska JX, Wolfe AM (2009) On the (Non)Evolution of H I Gas in Galaxies Over Cosmic Time. ApJ696:1543–1547, DOI 10.1088/0004-637X/696/2/1543, 0811.2003

Prochaska JX, Howk JC, O'Meara JM, Tytler D, Wolfe AM, Kirkman D, Lubin D, Suzuki N (2002) The UCSD HIRES/Keck I Damped Lyα Abundance Database. III. An Empirical Study of Photoionization in the Damped Lyα System toward GB 1759+7539. ApJ571:693–711, DOI 10.1086/340066, astro-ph/0202140

Prochaska JX, Sheffer Y, Perley DA, Bloom JS, Lopez LA, Dessauges-Zavadsky M, Chen HW, Filippenko AV, Ganeshalingam M, Li W, Miller AA, Starr D (2009) The First Positive Detection of Molecular Gas in a GRB Host Galaxy. ApJL691:L27–L32, DOI 10.1088/0004-637X/691/1/L27, 0901.0556

Putman ME, Peek JEG, Joung MR (2012) Gaseous Galaxy Halos. ARA&A50:491–529, DOI 10.1146/annurev-astro-081811-125612, 1207.4837

Rafelski M, Wolfe AM, Chen HW (2011) Star Formation from DLA Gas in the Outskirts of Lyman Break Galaxies at z ˜ 3. ApJ736:48, DOI 10.1088/0004-637X/736/1/48, 1011.6390

Rafelski M, Wolfe AM, Prochaska JX, Neeleman M, Mendez AJ (2012) Metallicity Evolution of Damped Lyα Systems Out to z ˜ 5. ApJ755:89, DOI 10.1088/0004-637X/755/2/89, 1205.5047

Rafelski M, Neeleman M, Fumagalli M, Wolfe AM, Prochaska JX (2014) The Rapid Decline in Metallicity of Damped Lyα Systems at z ˜ 5. ApJL782:L29, DOI 10.1088/2041-8205/782/2/L29, 1310.6042

Rafelski M, Gardner JP, Fumagalli M, Neeleman M, Teplitz HI, Grogin N, Koekemoer AM, Scarlata C (2016) The Star Formation Rate Efficiency of Neutral Atomic-dominated Hydrogen Gas in the Outskirts of Star-forming Galaxies from z ˜ 1 to z ˜3. ApJ825:87, DOI 10.3847/0004-637X/825/2/87, 1604.08597

Rao SM, Nestor DB, Turnshek DA, Lane WM, Monier EM, Bergeron J (2003) Low-Redshift Damped Lyα Galaxies toward the Quasars B2 0827+243, PKS 0952+179, PKS 1127-145, and PKS 1629+120. ApJ595:94–108, DOI 10.1086/377331, astro-ph/0211297

Rao SM, Turnshek DA, Nestor DB (2006) Damped Lyα Systems at z<1.65: The Expanded Sloan Digital Sky Survey Hubble Space Telescope Sample. ApJ636:610–630, DOI 10.1086/498132, astro-ph/0509469

Rao SM, Belfort-Mihalyi M, Turnshek DA, Monier EM, Nestor DB, Quider A (2011) A ground-based imaging study of galaxies causing damped Lyman α (DLA), sub-DLA and Lyman limit system absorption in quasar spectra. MNRAS416:1215–1249, DOI 10.1111/j.1365-2966.2011.19119.x, 1103.4047

Rauch M (1998) The Lyman Alpha Forest in the Spectra of QSOs. ARA&A36:267–316, DOI 10.1146/annurev.astro.36.1.267, astro-ph/9806286

Rauch M, Sargent WLW, Womble DS, Barlow TA (1996) Temperature and Kinematics of C IV Absorption Systems. ApJL467:L5, DOI 10.1086/310187, astro-ph/9606041

Reddy NA, Pettini M, Steidel CC, Shapley AE, Erb DK, Law DR (2012) The Characteristic Star Formation Histories of Galaxies at Redshifts z ˜ 2-7. ApJ754:25, DOI 10.1088/0004-637X/754/1/25, 1205.0555

Rémy-Ruyer A, Madden SC, Galliano F, Galametz M, Takeuchi TT, Asano RS, Zhukovska S, Lebouteiller V, Cormier D, Jones A, Bocchio M, Baes M, Bendo GJ, Boquien M, Boselli A, DeLooze I, Doublier-Pritchard V, Hughes T, Karczewski OŁ, Spinoglio L (2014) Gas-to-dust mass ratios in local galaxies over a 2 dex metallicity range. A&A563:A31, DOI 10.1051/0004-6361/201322803, 1312.3442

Richards GT, Strauss MA, Fan X, Hall PB, Jester S, Schneider DP, Vanden Berk DE, Stoughton C, Anderson SF, Brunner RJ, Gray J, Gunn JE, Ivezić Ž, Kirkland MK, Knapp GR, Loveday J, Meiksin A, Pope A, Szalay AS, Thakar AR, Yanny B, York DG, Barentine JC, Brewington HJ, Brinkmann J, Fukugita M, Harvanek M, Kent SM, Kleinman SJ, Krzesiński J, Long DC, Lupton RH, Nash T, Neilsen EH Jr, Nitta A, Schlegel DJ, Snedden SA (2006) The Sloan Digital Sky Survey Quasar Survey: Quasar Luminosity Function from Data Release 3. AJ131:2766–2787, DOI 10.1086/503559, astro-ph/0601434

Rigby JR, Charlton JC, Churchill CW (2002) The Population of Weak Mg II Absorbers. II. The Properties of Single-Cloud Systems. ApJ565:743–761, DOI 10.1086/324723, astro-ph/0110191

Rubin KHR, Prochaska JX, Ménard B, Murray N, Kasen D, Koo DC, Phillips AC (2011) Low-ionization Line Emission from a Starburst Galaxy: A New Probe of a Galactic-scale Outflow. ApJ728:55, DOI 10.1088/0004-637X/728/1/55, 1008.3397

Rubin KHR, Hennawi JF, Prochaska JX, Simcoe RA, Myers A, Lau MW (2015) Dissecting the Gaseous Halos of $z\sim2$ Damped Lyα Systems with Close Quasar Pairs. ApJ808:38, DOI 10.1088/0004-637X/808/1/38, 1411.6016

Salim S, Rich RM (2010) Star Formation Signatures in Optically Quiescent Early-type Galaxies. ApJL714:L290–L294, DOI 10.1088/2041-8205/714/2/L290, 1004.2041

Sánchez SF, Rosales-Ortega FF, Iglesias-Páramo J, Mollá M, Barrera-Ballesteros J, Marino RA, Pérez E, Sánchez-Blazquez P, González Delgado R, Cid Fernandes R, de Lorenzo-Cáceres A, Mendez-Abreu J, Galbany L, Falcon-Barroso J, Miralles-Caballero D, Husemann B, García-Benito R, Mast D, Walcher CJ, Gil de Paz A, García-Lorenzo B, Jungwiert B, Vílchez JM, Jílková L, Lyubenova M, Cortijo-Ferrero C, Díaz AI, Wisotzki L, Márquez I, Bland-Hawthorn J, Ellis S, van de Ven G, Jahnke K, Papaderos P, Gomes JM, Mendoza MA, López-Sánchez ÁR (2014) A characteristic oxygen abundance gradient in galaxy disks unveiled with CALIFA. A&A563:A49, DOI 10.1051/0004-6361/201322343, 1311.7052

Sánchez-Ramírez R, Ellison SL, Prochaska JX, Berg TAM, López S, D'Odorico V, Becker GD, Christensen L, Cupani G, Denney KD, Pâris I, Worseck G, Gorosabel J (2016) The evolution of neutral gas in damped Lyman α systems from the XQ-100 survey. MNRAS456:4488–4505, DOI 10.1093/mnras/stv2732, 1511.05003

Savage BD, Sembach KR (1996) Interstellar Abundances from Absorption-Line Observations with the Hubble Space Telescope. ARA&A34:279–330, DOI 10.1146/annurev.astro.34.1.279

Savage BD, Sembach KR, Tripp TM, Richter P (2002) Far Ultraviolet Spectroscopic Explorer and Space Telescope Imaging Spectrograph Observations of Intervening O VI Absorption Line Systems in the Spectrum of PG 0953+415. ApJ564:631–649, DOI 10.1086/324288

Schechter P (1976) An analytic expression for the luminosity function for galaxies. ApJ203:297–306, DOI 10.1086/154079

Schmidt M (1959) The Rate of Star Formation. ApJ129:243, DOI 10.1086/146614

Serra P, Oosterloo T, Morganti R, Alatalo K, Blitz L, Bois M, Bournaud F, Bureau M, Cappellari M, Crocker AF, Davies RL, Davis TA, de Zeeuw PT, Duc PA, Emsellem E, Khochfar S, Krajnović D, Kuntschner H, Lablanche PY, McDermid RM, Naab T, Sarzi M, Scott N, Trager SC, Weijmans AM, Young LM (2012) The ATLAS^{3D} project - XIII. Mass and morphology of H I in early-type galaxies as a function of environment. MNRAS422:1835–1862, DOI 10.1111/j.1365-2966.2012.20219.x, 1111.4241

Shen S, Madau P, Guedes J, Mayer L, Prochaska JX, Wadsley J (2013) The Circumgalactic Medium of Massive Galaxies at z ˜ 3: A Test for Stellar Feedback, Galactic Outflows, and Cold Streams. ApJ765:89, DOI 10.1088/0004-637X/765/2/89, 1205.0270

Simcoe RA (2011) The Carbon Content of Intergalactic Gas at z = 4.25 and Its Evolution toward z = 2.4. ApJ738:159, DOI 10.1088/0004-637X/738/2/159, 1106.2810

Som D, Kulkarni VP, Meiring J, York DG, Péroux C, Lauroesch JT, Aller MC, Khare P (2015) Hubble Space Telescope Observations of Sub-damped Lyα Absorbers at z $<$ 0.5, and Implications for Galaxy Chemical Evolution. ApJ806:25, DOI 10.1088/0004-637X/806/1/25, 1502.01989

Steidel CC, Kollmeier JA, Shapley AE, Churchill CW, Dickinson M, Pettini M (2002) The Kinematic Connection between absorbing Gas toward QSOs and Galaxies at Intermediate Redshift. ApJ570:526–542, DOI 10.1086/339792, astro-ph/0201353

Steidel CC, Erb DK, Shapley AE, Pettini M, Reddy N, Bogosavljević M, Rudie GC, Rakic O (2010) The Structure and Kinematics of the Circumgalactic Medium from Far-ultraviolet Spectra of z ˜= 2-3 Galaxies. ApJ717:289–322, DOI 10.1088/0004-637X/717/1/289, 1003.0679

Stocke JT, Penton SV, Danforth CW, Shull JM, Tumlinson J, McLin KM (2006) The Galaxy Environment of O VI Absorption Systems. ApJ641:217–228, DOI 10.1086/500386, astro-ph/0509822

Stocke JT, Keeney BA, Danforth CW, Shull JM, Froning CS, Green JC, Penton SV, Savage BD (2013) Characterizing the Circumgalactic Medium of Nearby Galaxies with HST/COS and HST/STIS Absorption-line Spectroscopy. ApJ763:148, DOI 10.1088/0004-637X/763/2/148, 1212.5658

Straka LA, Noterdaeme P, Srianand R, Nutalaya S, Kulkarni VP, Khare P, Bowen D, Bishof M, York DG (2015) Galactic nebular lines in the fibre spectra of background QSOs: reaching a hundred QSO-galaxy pairs with spectroscopic and photometric measurements. MNRAS447:3856–3872, DOI 10.1093/mnras/stu2739, 1412.6661

Swaters RA, van Albada TS, van der Hulst JM, Sancisi R (2002) The Westerbork HI survey of spiral and irregular galaxies. I. HI imaging of late-type dwarf galaxies. A&A390:829–861, DOI 10.1051/0004-6361:20011755, astro-ph/0204525

Tacconi LJ, Neri R, Genzel R, Combes F, Bolatto A, Cooper MC, Wuyts S, Bournaud F, Burkert A, Comerford J, Cox P, Davis M, Förster Schreiber NM, García-Burillo S, Gracia-Carpio J, Lutz D, Naab T, Newman S, Omont A, Saintonge A, Shapiro Griffin K, Shapley A, Sternberg A, Weiner B (2013) Phibss: Molecular Gas Content and Scaling Relations in z ˜ 1-3 Massive, Main-sequence Star-forming Galaxies. ApJ768:74, DOI 10.1088/0004-637X/768/1/74, 1211.5743

Tremonti CA, Heckman TM, Kauffmann G, Brinchmann J, Charlot S, White SDM, Seibert M, Peng EW, Schlegel DJ, Uomoto A, Fukugita M, Brinkmann J (2004) The Origin of the Mass-Metallicity Relation: Insights from 53,000 Star-forming Galaxies in the Sloan Digital Sky Survey. ApJ613:898–913, DOI 10.1086/423264, astro-ph/0405537

Tripp TM, Giroux ML, Stocke JT, Tumlinson J, Oegerle WR (2001) The Ionization and Metallicity of the Intervening O VI Absorber at z=0.1212 in the Spectrum of H1821+643. ApJ563:724–735, DOI 10.1086/323965, astro-ph/0108371

Tumlinson J (2006) Chemical Evolution in Hierarchical Models of Cosmic Structure. I. Constraints on the Early Stellar Initial Mass Function. ApJ641:1–20, DOI 10.1086/500383, astro-ph/0507442

Tumlinson J, Shull JM, Rachford BL, Browning MK, Snow TP, Fullerton AW, Jenkins EB, Savage BD, Crowther PA, Moos HW, Sembach KR, Sonneborn G, York DG (2002) A Far Ultraviolet Spectroscopic Explorer Survey of Interstellar Molecular Hydrogen in the Small and Large Magellanic Clouds. ApJ566:857–879, DOI 10.1086/338112, astro-ph/0110262

Tumlinson J, Prochaska JX, Chen HW, Dessauges-Zavadsky M, Bloom JS (2007) Missing Molecular Hydrogen and the Physical Conditions of GRB Host Galaxies. ApJ668:667–673, DOI 10.1086/521294, astro-ph/0703666

Tumlinson J, Thom C, Werk JK, Prochaska JX, Tripp TM, Weinberg DH, Peeples MS, O'Meara JM, Oppenheimer BD, Meiring JD, Katz NS, Davé R, Ford AB, Sembach KR (2011) The Large, Oxygen-Rich Halos of Star-Forming Galaxies Are a Major Reservoir of Galactic Metals. Science 334:948, DOI 10.1126/science.1209840, 1111.3980

Tumlinson J, Thom C, Werk JK, Prochaska JX, Tripp TM, Katz N, Davé R, Oppenheimer BD, Meiring JD, Ford AB, O'Meara JM, Peeples MS, Sembach KR, Weinberg DH (2013) The COS-Halos Survey: Rationale, Design, and a Census of Circumgalactic Neutral Hydrogen. ApJ777:59, DOI 10.1088/0004-637X/777/1/59, 1309.6317

van Zee L, Salzer JJ, Haynes MP, O'Donoghue AA, Balonek TJ (1998) Spectroscopy of Outlying H II Regions in Spiral Galaxies: Abundances and Radial Gradients. AJ116:2805–2833, DOI 10.1086/300647, astro-ph/9808315

Verdes-Montenegro L, Yun MS, Williams BA, Huchtmeier WK, Del Olmo A, Perea J (2001) Where is the neutral atomic gas in Hickson groups? A&A377:812–826, DOI 10.1051/0004-6361:20011127, astro-ph/0108223

Verheijen M, van Gorkom JH, Szomoru A, Dwarakanath KS, Poggianti BM, Schiminovich D (2007) WSRT Ultradeep Neutral Hydrogen Imaging of Galaxy Clusters at z ˜ 0.2: A Pilot Survey of Abell 963 and Abell 2192. ApJL668:L9–L13, DOI 10.1086/522621, 0708.3853

Verheijen MAW, Sancisi R (2001) The Ursa Major cluster of galaxies. IV. HI synthesis observations. A&A370:765–867, DOI 10.1051/0004-6361:20010090, astro-ph/0101404

Viegas SM (1995) Abundances at high redshift: ionization correction factors. MNRAS276:268–272, DOI 10.1093/mnras/276.1.268

Vladilo G, Centurión M, Bonifacio P, Howk JC (2001) Ionization Properties and Elemental Abundances in Damped Lyα Systems. ApJ557:1007–1020, DOI 10.1086/321650, astro-ph/0104298

Walter F, Brinks E, de Blok WJG, Bigiel F, Kennicutt RC Jr, Thornley MD, Leroy A (2008) THINGS: The H I Nearby Galaxy Survey. AJ136:2563-2647, DOI 10.1088/0004-6256/136/6/2563, 0810.2125

Walter F, Decarli R, Sargent M, Carilli C, Dickinson M, Riechers D, Ellis R, Stark D, Weiner B, Aravena M, Bell E, Bertoldi F, Cox P, Da Cunha E, Daddi E, Downes D, Lentati L, Maiolino R, Menten KM, Neri R, Rix HW, Weiss A (2014) A Molecular Line Scan in the Hubble Deep Field North: Constraints on the CO Luminosity Function and the Cosmic H_2 Density. ApJ782:79, DOI 10.1088/0004-637X/782/2/79, 1312.6365

Warren SJ, Møller P, Fall SM, Jakobsen P (2001) NICMOS imaging search for high-redshift damped Lyα galaxies. MNRAS326:759–773, DOI 10.1046/j.1365-8711.2001.04629.x, astro-ph/0105032

Werk JK, Prochaska JX, Thom C, Tumlinson J, Tripp TM, O'Meara JM, Peeples MS (2013) The COS-Halos Survey: An Empirical Description of Metal-line Absorption in the Low-redshift Circumgalactic Medium. ApJS204:17, DOI 10.1088/0067-0049/204/2/17, 1212.0558

Werk JK, Prochaska JX, Tumlinson J, Peeples MS, Tripp TM, Fox AJ, Lehner N, Thom C, O'Meara JM, Ford AB, Bordoloi R, Katz N, Tejos N, Oppenheimer BD, Davé R, Weinberg DH (2014) The COS-Halos Survey: Physical Conditions and Baryonic Mass in the Low-redshift Circumgalactic Medium. ApJ792:8, DOI 10.1088/0004-637X/792/1/8, 1403.0947

Westmeier T, Brüns C, Kerp J (2008) Relics of structure formation: extra-planar gas and high-velocity clouds around the Andromeda Galaxy. MNRAS390:1691–1709, DOI 10.1111/j.1365-2966.2008.13858.x, 0808.3611

Wolfe AM, Chen HW (2006) Searching for Low Surface Brightness Galaxies in the Hubble Ultra Deep Field: Implications for the Star Formation Efficiency in Neutral Gas at z˜3. ApJ652:981–993, DOI 10.1086/507574, astro-ph/0608040

Wolfe AM, Turnshek DA, Smith HE, Cohen RD (1986) Damped Lyman-alpha absorption by disk galaxies with large redshifts. I - The Lick survey. ApJS61:249–304, DOI 10.1086/191114

Wolfe AM, Lanzetta KM, Foltz CB, Chaffee FH (1995) The Large Bright QSO Survey for Damped LY alpha Absorption Systems. ApJ454:698, DOI 10.1086/176523

Wolfe AM, Gawiser E, Prochaska JX (2005) Damped Ly α Systems. ARA&A43:861–918, DOI 10.1146/annurev.astro.42.053102.133950, astro-ph/0509481

Wolfire MG, Tielens AGGM, Hollenbach D, Kaufman MJ (2008) Chemical Rates on Small Grains and PAHs: C^+ Recombination and H_2 Formation. ApJ680:384-397, DOI 10.1086/587688, 0803.0138

Wong T, Blitz L (2002) The Relationship between Gas Content and Star Formation in Molecule-rich Spiral Galaxies. ApJ569:157–183, DOI 10.1086/339287, astro-ph/0112204

Wright SA, Larkin JE, Law DR, Steidel CC, Shapley AE, Erb DK (2009) Dynamics of Galactic Disks and Mergers at z ˜ 1.6: Spatially Resolved Spectroscopy with Keck Laser Guide Star Adaptive Optics. ApJ699:421–440, DOI 10.1088/0004-637X/699/1/421, 0810.5599

Wuyts E, Wisnioski E, Fossati M, Förster Schreiber NM, Genzel R, Davies R, Mendel JT, Naab T, Röttgers B, Wilman DJ, Wuyts S, Bandara K, Beifiori A,

Belli S, Bender R, Brammer GB, Burkert A, Chan J, Galametz A, Kulkarni SK, Lang P, Lutz D, Momcheva IG, Nelson EJ, Rosario D, Saglia RP, Seitz S, Tacconi LJ, Tadaki Ki, Übler H, van Dokkum P (2016) The Evolution of Metallicity and Metallicity Gradients from z = 2.7 to 0.6 with KMOS^{3D}. ApJ827:74, DOI 10.3847/0004-637X/827/1/74, 1603.01139

Wyder TK, Martin DC, Barlow TA, Foster K, Friedman PG, Morrissey P, Neff SG, Neill JD, Schiminovich D, Seibert M, Bianchi L, Donas J, Heckman TM, Lee YW, Madore BF, Milliard B, Rich RM, Szalay AS, Yi SK (2009) The Star Formation Law at Low Surface Density. ApJ696:1834–1853, DOI 10.1088/0004-637X/696/2/1834, 0903.3015

York DG, Adelman J, Anderson JE Jr, Anderson SF, Annis J, Bahcall NA, Bakken JA, Barkhouser R, Bastian S, Berman E, Boroski WN, Bracker S, Briegel C, Briggs JW, Brinkmann J, Brunner R, Burles S, Carey L, Carr MA, Castander FJ, Chen B, Colestock PL, Connolly AJ, Crocker JH, Csabai I, Czarapata PC, Davis JE, Doi M, Dombeck T, Eisenstein D, Ellman N, Elms BR, Evans ML, Fan X, Federwitz GR, Fiscelli L, Friedman S, Frieman JA, Fukugita M, Gillespie B, Gunn JE, Gurbani VK, de Haas E, Haldeman M, Harris FH, Hayes J, Heckman TM, Hennessy GS, Hindsley RB, Holm S, Holmgren DJ, Huang Ch, Hull C, Husby D, Ichikawa SI, Ichikawa T, Ivezić Ž, Kent S, Kim RSJ, Kinney E, Klaene M, Kleinman AN, Kleinman S, Knapp GR, Korienek J, Kron RG, Kunszt PZ, Lamb DQ, Lee B, Leger RF, Limmongkol S, Lindenmeyer C, Long DC, Loomis C, Loveday J, Lucinio R, Lupton RH, MacKinnon B, Mannery EJ, Mantsch PM, Margon B, McGehee P, McKay TA, Meiksin A, Merelli A, Monet DG, Munn JA, Narayanan VK, Nash T, Neilsen E, Neswold R, Newberg HJ, Nichol RC, Nicinski T, Nonino M, Okada N, Okamura S, Ostriker JP, Owen R, Pauls AG, Peoples J, Peterson RL, Petravick D, Pier JR, Pope A, Pordes R, Prosapio A, Rechenmacher R, Quinn TR, Richards GT, Richmond MW, Rivetta CH, Rockosi CM, Ruthmansdorfer K, Sandford D, Schlegel DJ, Schneider DP, Sekiguchi M, Sergey G, Shimasaku K, Siegmund WA, Smee S, Smith JA, Snedden S, Stone R, Stoughton C, Strauss MA, Stubbs C, SubbaRao M, Szalay AS, Szapudi I, Szokoly GP, Thakar AR, Tremonti C, Tucker DL, Uomoto A, Vanden Berk D, Vogeley MS, Waddell P, Wang Si, Watanabe M, Weinberg DH, Yanny B, Yasuda N, SDSS Collaboration (2000) The Sloan Digital Sky Survey: Technical Summary. AJ120:1579–1587, DOI 10.1086/301513, astro-ph/0006396

Yun MS, Ho PTP, Lo KY (1994) A high-resolution image of atomic hydrogen in the M81 group of galaxies. Nature372:530–532, DOI 10.1038/372530a0

Zahedy FS, Chen HW, Rauch M, Wilson ML, Zabludoff A (2016) Probing the cool interstellar and circumgalactic gas of three massive lensing galaxies at z = 0.4-0.7. MNRAS458:2423–2442, DOI 10.1093/mnras/stw484, 1510.04307

Zaritsky D, Kennicutt RC Jr, Huchra JP (1994) H II regions and the abundance properties of spiral galaxies. ApJ420:87–109, DOI 10.1086/173544

Zwaan MA, Prochaska JX (2006) Where Is the Molecular Hydrogen in Damped Lyα Absorbers? ApJ643:675–679, DOI 10.1086/503191, astro-ph/0601655

Zwaan MA, van der Hulst JM, Briggs FH, Verheijen MAW, Ryan-Weber EV (2005) Reconciling the local galaxy population with damped Lyman α cross-sections and metal abundances. MNRAS364:1467–1487, DOI 10.1111/j.1365-2966.2005.09698.x, astro-ph/0510127